ChemSusChem

Supporting Information

Aquivion-Based Spray Freeze-Dried Composite Materials for the Cascade Production of γ-Valerolactone

Alessandro Allegri, Anna Saotta, Francesca Liuzzi, Enrica Gianotti, Geo Paul, Alice S. Cattaneo, Claudio Oldani, Andrea Brigliadori, Ilaria Zanoni, Giuseppe Fornasari, Nikolaos Dimitratos, and Stefania Albonetti*

SUPPORTING INFORMATION

Supporting Information

69451 Weinheim, Germany

Aquivion-based spray freeze-dried composite materials for the cascade production of γ-valerolactone

Alessandro Allegri, Anna Saotta, Francesca Liuzzi, Enrica Gianotti, Geo Paul, Alice S. Cattaneo, Claudio Oldani, Andrea Brigliadori, Ilaria Zanoni, Giuseppe Fornasari, Nikolaos Dimitratos and Stefania Albonetti*

Abstract: The development of multifunctional catalysts is a necessary step to effectively carry out one-pot cascade reactions, such as that from furfural to γ-valerolactone. This research effort faces the challenge posed by the intrinsic limit of how many kinds of catalytic sites a single material can bear. In this work, the application of Spray-Freeze Drying (SFD) as a synthetic technique for the preparation of a wide range of innovative composite multi-functional catalysts is reported. Herein we show that by the proper combination of Aquivion as a highly active Brønsted acid catalyst and metal oxides as both support materials and Lewis acids (LAS) enable to achieve highly unique efficient and effective dual acid composite catalysts that are able to carry out the cascade reaction from furfural to γ-valerolactone. The dual catalytic system comprised of Aq/ZrO_2 with 30% polymer content prepared via spray-freeze drying) exhibited GVL yields of 25% after only 2 h at 180 °C and a remarkably high productivity of 4470 μmol_{GVL} g_{Cat}^{-1} h^{-1}, one of the highest reported results. Mechanistic studies based on experimental and advanced characterisation and spectroscopic techniques, such as, SEM, TEM, ^{15}N MAS NMR and ^{19}F MAS NMR indicate that activity arises from the proper tuning of BAS/LAS (Brønsted Acid Site/Lewis Acid Site) acidic properties with multifunctional acidic properties.

DOI: 10.1002/anie.2021XXXXX

Table of Contents

Table of Entries

SUPPORTING INFORMATION

SUPPORTING INFORMATION

Abbreviations

AnL: Angelica Lactones;
BAS: Brønsted Acid Sites;
CTH: Catalytic Transfer Hydrogenation;
DFE: Difurfuryl Ether (2,2'-(oxybis(methylene))difuran);
DFM: Difuryl Methane (di(furan-2-yl)methane);
EL: Ethyl Levulinate;
FAL: Furfuryl Alcohol;
FEE: Furfuryl Ethyl Ether;
FPE: Furfuryl Isopropyl Ether;
FU: Furfural;
GVL: Gamma-Valerolactone;
IPL: Isopropyl Levulinate;
LAS: Lewis Acid Sites;
PrL: Propyl Levulinate;
SFD: Spray Freeze-Drying;
SSA: Specific Surface Area;
TIPP: 4,5,5-triisopropoxypentanone;

Experimental Procedures

Spray Freeze-Drying

The spray freeze-drying of the composites requires the preparation of a water suspension of the phases involved in the synthesis with a total concentration of solids of 20 wt%. While Aquivion only required dilution before being added dropwise to the water suspension of the metal oxide that is to be part of the final composite, the second component required better control.
In the case of silica Ludox HS-40 water suspension, acidification was required to remove the stabilising sodium ions on its surface in order to promote coagulation after the spray process. This was achieved adding Dowex 50W X8 proton exchange resin under vigorous stirring and monitoring the pH. Once the pH value reached 4, the resin was removed via filtration to leave the silica suspension ready for mixing with Aquivion.
In the case of zirconia and titania, the oxidic powder was suspended in water, then the pH was measured to ensure that it was at or below 4. If necessary, small corrections could be made adding small amounts of 0.1M HCl water solution. The suspension was then subjected to 15 min of sonication to properly disperse the powder.
Once the oxide suspension was properly treated according to the previous procedures, Aquivion was added dropwise under vigorous stirring, then the mixed suspension was transferred into a polypropylene bottle. Zirconia milling balls (5mm diameter) were added, then the suspension was subjected to 24h of ball milling. After 24h, the milling balls were removed, and the ζ-potential of the suspension was measured to ensure that the heterocoagulation of the phases was properly achieved. The suspension was then utilised for the spray-freeze drying.
The spray-freeze drying process was carried out in a Lab-scale Granulator LS-2 (PowderPro AB), as represented in **Figure S1**. The suspension was co-fed to a nozzle along with a nitrogen flow to achieve proper atomisation, then directed onto a liquid nitrogen bath to instantly freeze the droplets into solid granules. The frozen granules were then transferred to a lyophilizer (LYO GT 2, SRK System Technik) to sublimate water.

The resulting materials were afterwards calcined under static air to ensure consolidation of the structure. A ramp of 2 °C/min was employed to reach the calcination temperature of 200 °C, which was then kept constant for 3 h, then cooled with a ramp of 10 °C/min down to room temperature.

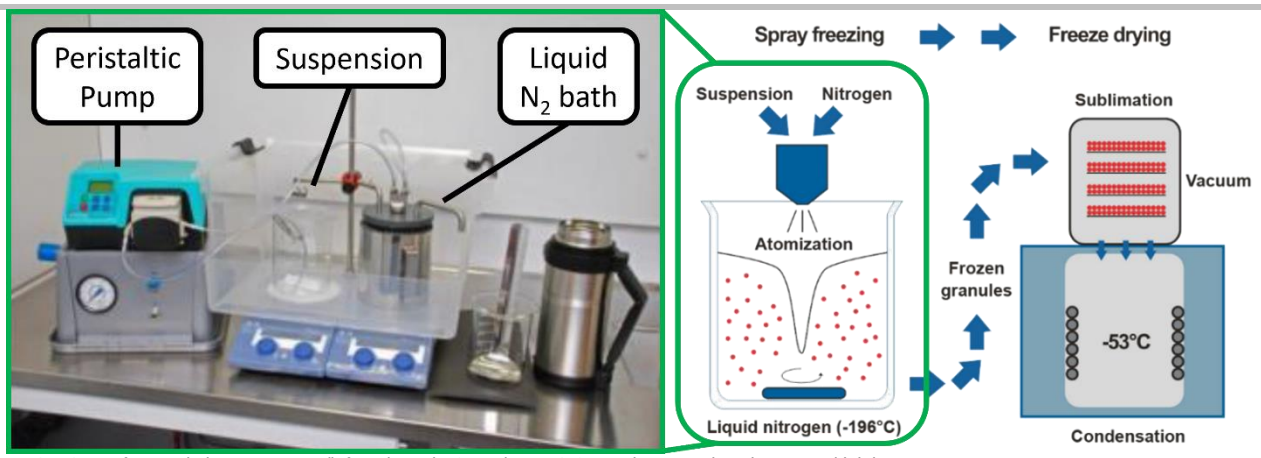

Figure S1. Spray freeze-drying apparatus (left, Lab-scale Granulator LS-2 PowderPro AB) and process (right).

ζ-potential measurement

ζ-potential of water suspensions of the employed phases and the mixed suspensions was carried out in a Zetasizer Nano ZSP (Malvern Instruments) DLS/ELS instrument, automatically varying the pH of the suspension with addition of either HCl or KOH 0.1M water solutions. The measurement of ζ-potential was made via electrophoretic mobility in a Smoluchowski cell.

Scanning Electron Microscopy

The spray freeze-dried composite materials were observed via a field emission scanning electron microscope (FESEM, Carl Zeiss Sigma NTS). Elemental analysis was performed using an energy dispersive X-ray microanalyzer (EDX, INCA Energy 300, Oxford Instruments). The observed samples were fixed to aluminium stubs with conductive adhesive tape.

N_2 Adsorption/Desorption Porosimetry

The textural properties of the samples were measured from N_2 adsorption-desorption isotherms at 77 K on a Micromeritics ASAP 2020 surface area analyser. Samples were previously outgassed for 30 min at 150 °C and 15 μmHg, and then held for 30 min at 200-240 °C. Specific surface area values were obtained by multi-point BET equation while average diameter of the pores and pore volumes using BJH method.

Thermogravimetric Analysis

Thermal behaviour and polymer content of the composite materials was assessed by thermogravimetric analysis in a TA Instruments Q600 TGA instrument. Samples were loaded in an alumina sample holder and heated with a ramp of 10 °C/min up to 700 °C, then held for 30min of isothermal step. The dry weight of the samples was assumed to be the weight measured at 200 °C, a temperature high enough to ensure water desorption even from the acid sites, but low enough to avoid any modification of the catalysts. The polymer content of each sample was calculated as follows:

$$y_{Polymer} = \frac{(m_{200\,°C} - m_{700\,°C})}{m_{200\,°C}}$$

Solid-State Magic Angle Spinning Nuclear Magnetic Resonance

The density of Aquivion Brønsted acid sites was measured both on the pure polymer and on the composite catalysts via solid state NMR. ^{19}F MAS NMR spectra were recorded with a Bruker AVANCE III 400 WB spectrometer, equipped with a 4 mm standard probe spinning at 28 kHz. Example spectra are reported in **Figure S2**. The spectra are characterised by one main signal at −122 ppm associated with the -$(CF_2)_n$- units of the main polymeric chain, while the smaller signals are associated with the side chains: CF at −138 ppm; OCF_2 at −79 ppm; CF2 bound to the sulfonic groups at −118 ppm.[1] Marked with asterisks in the figure are the spinning sidebands of the main signals, caused by an insufficient rotating speed of the probe, which causes ^{19}F-^{19}F homonuclear coupling. These are characterized by a distance from the main signal equal to the spinning frequency, which marks them clearly as artifacts. The sample holder and rotor are both fluorinated, giving rise to the signals at −104 ppm and −133 ppm. The intensity of these peaks depends on the amount of fluorine in the sample, making them barely noticeable when analysing pure Aquivion, while their presence is marked in the spectra of composite catalysts. From the ratio between the area of the signal of the side chains (in particular, the signal of the OCF_2 groups at −79 ppm) and the area of the signal of the main chains (at −122 ppm) it is possible to calculate the equivalent weight of the polymer and its acid loading.

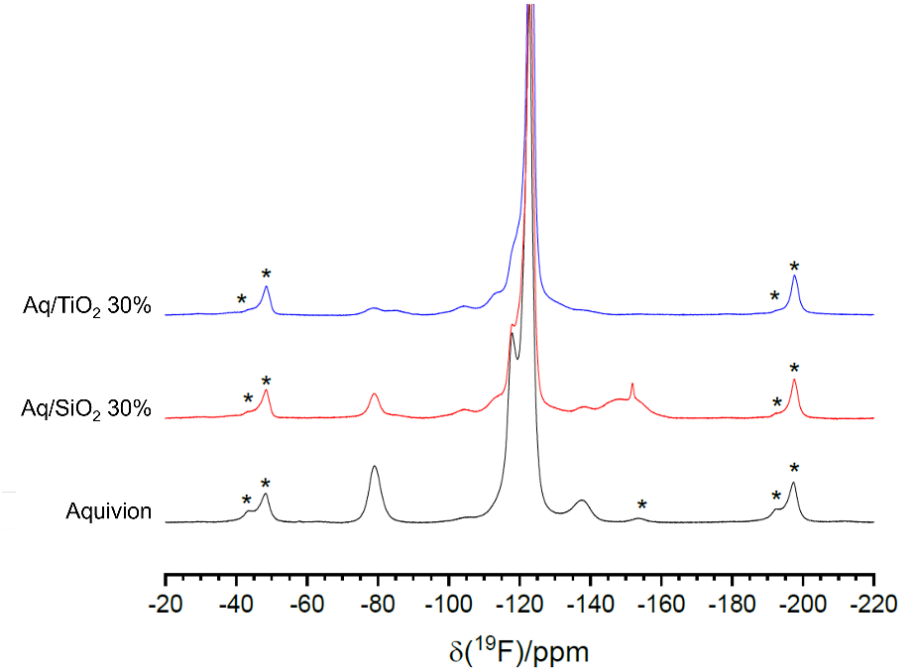

Figure S2. Example ^{19}F one pulse MAS NMR spectra obtained on pure Aquivion (in black) and composite materials with silica (in red) and titania (in blue). Asterisks mark the spinning side bands of the main signals.

Additional solid-state NMR spectroscopic measurements were carried out on a Bruker Avance III 500 spectrometer and a wide bore 11.75 Tesla magnet with operational frequencies for ^{1}H, ^{15}N and ^{13}C of 500.13, 50.69 and 125.77 MHz, respectively. A 4 mm triple resonance probe in double resonance mode with MAS was employed in all the experiments. The Lewis and Brønsted acidic features of the samples were qualitatively and quantitatively determined via pyridine adsorption at 25°C, followed by ^{15}N and ^{1}H MAS NMR spectroscopy. Prior to the acquisition of the NMR spectra, samples were packed in a 4 mm rotor and pre-treated at 180 °C (temperature of the catalytic test) for 2 h in a vacuum line (below 10^{-5} mbar) and then cooled to room temperature followed by pyridine adsorption at 20 mbar for 1 h. Subsequently, the pyridine-loaded samples were evacuated at room temperature for 30 minutes to remove physisorbed pyridine. For the calculation of the ratio of the Lewis and Brønsted acid sites, the integral intensities of the pyridine signals from the ^{15}N MAS NMR spectra were used.

^{1}H, ^{15}N and ^{13}C MAS NMR spectra were recorded using a single-pulse excitation experiment with pulse durations of 2.5, 8 and 3.8 µs, as well as 16, 20k and 2k transients, respectively. During the^{15}N and ^{13}C MAS NMR experiments proton decoupling was applied. For the ^{13}C cross-polarization (CP) magic angle spinning (MAS) experiments, the proton radio frequencies (RF) of 55 and 28 kHz were used for initial excitation and decoupling, respectively. During the CP period the ^{1}H RF field was ramped using 100 increments, whereas the ^{13}C RF field was maintained at a constant level using a contact time of 5 ms. During the acquisition, the protons were decoupled from the carbons by using a Spinal-64 decoupling scheme. A moderate ramped RF field of 55 kHz was used for spin locking, while the carbon RF field was matched to obtain optimal signal (40 kHz). Spectra were recorded with a spectral width of 50 kHz and 10k transients were accumulated at 298 K. All chemical shifts are reported using δ scale and are externally referenced to TMS at 0 ppm.

Furfural Distillation

While the other chemicals were used as supplied, without any further purification, the high propensity of furfural for the formation of oligomers made a purification step necessary before being used as a reaction substrate.
The distillation of furfural was carried out via the formation of an azeotrope with water. A 65 wt% water / 35 wt% furfural mixture was placed in a round bottom flask along and connected to a Vigreux column and a water condenser. The mixture was heated under stirring to its boiling point (98 °C) and the temperature was kept until the temperature in the flask reached 100 °C, signalling the complete depletion of furfural in the mixture. From the water condenser, the condensed azeotrope was collected in a separator funnel and allowed to cool until the two components separated, leaving a clear and almost colourless furfural phase on the bottom and a water phase on top. Purified furfural was collected, dried over sodium sulphate anhydrous and stored in a bottle with sodium sulphate and potassium hydroxide, in a nitrogen atmosphere.

Batch Reactions

Batch reactions were carried out in a 50 mL steel autoclave with both stirring and heating provided by an IKA RCT Basic magnetic stirrer through an aluminium mantle (**Figure S3**). The autoclave was loaded with 15 mL of isopropanol, 1mmol of substrate and the appropriate amount of water and catalyst, then sealed. The autoclave was then loaded with 15 bar of nitrogen and purged, repeating this process three times to ensure removal of air from inside. 10bar of nitrogen were then loaded to ensure that isopropanol does not evaporate in large quantities during heating. The loaded and sealed autoclave was then placed in the heating mantle and heated to the target temperature over 15min. The reaction time was measured when the thermocouple placed inside the autoclave registered less than 1 °C offset from the target temperature. At the end of reaction time, the autoclave was placed in an ice bath to quickly quench

the reaction. The reaction mixture was then accurately collected in a 25 mL volumetric flask, 20 µL of octane were added as internal standard. The reaction mixture was then diluted to the volume of the flask and analysed it via GC.

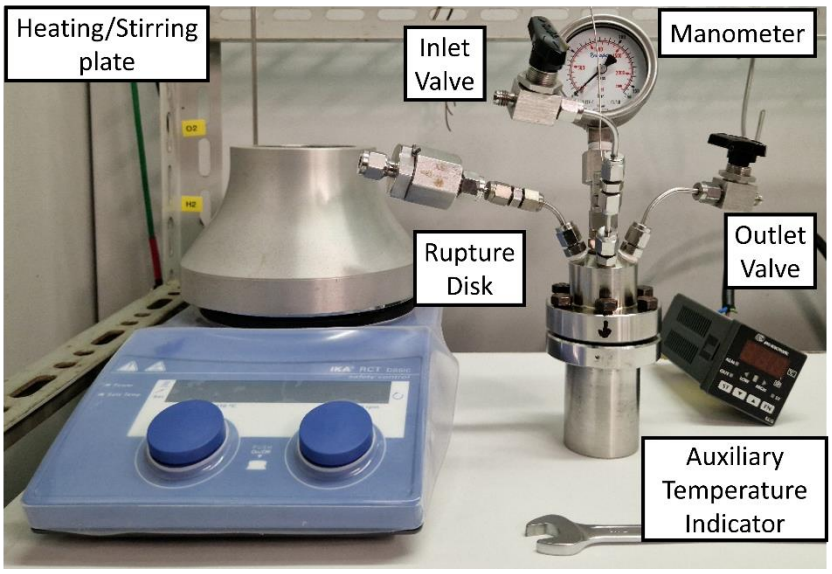

Figure S3. Autoclave employed for the batch catalytic reactions.

Products Quantification via Gas Chromatography

The post-reaction solutions were analysed in a Perkin-Elmer Clarus500 Gas Chromatograph equipped with an Agilent HP-5 column. 0.5 µL of solution were injected, with an injector temperature of 250 °C. The temperature of the oven containing the column was set at 50 °C for the first 2min of the analysis, then increased by 10 °C/min up to 250 °C and kept at 250 °C for the last two minutes. The instrument was equipped with an FID detector set at 250 °C, with a 50 mL/min flow of hydrogen and a 450 mL/min flow of air. A sample chromatogram is reported in **Figure S4**, with indicated all the main compounds observed in this study at their retention time.

The quantification of the reactant(s) and products was made via the calibration curves reported in **Figure S5**, obtained preparing solutions of different commercial standards at varying concentrations, with a constant amount of standard (octane). For each chromatogram, the possible variations in injection volume were offset dividing the area of each peak by the area of the peak associated with octane and dividing the moles of the substrate by the moles of the standard. The response factors for each species were assumed to be the slope of the linear fit of the obtained plots.

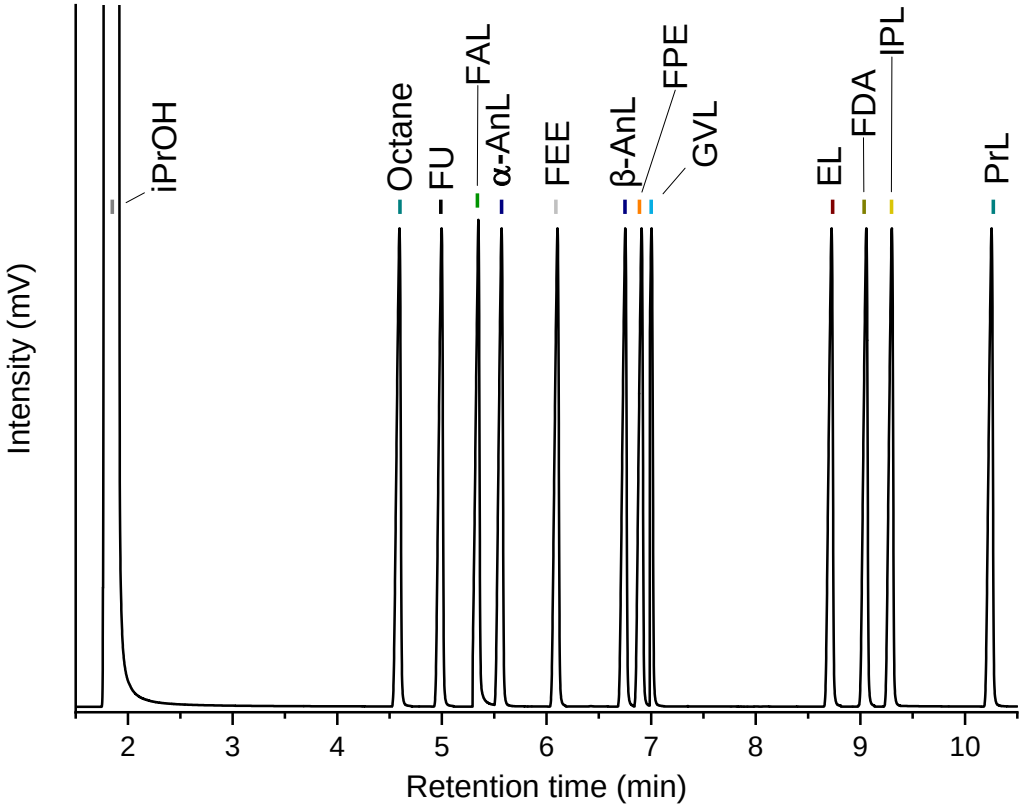

Figure S4. Sample chromatogram with the more commonly observed molecules. :iPrOH: isopropanol; FU: furfural; FAL: furfuryl alcohol; α/β-AnL: α/β-angelica lactone; FEE: furfuryl ethyl ether; FPE: furfuryl isopropyl ether; GVL: γ-valerolactone; EL: ethyl levulinate; FDA: furfural diisopropyl acetal; IPL: isopropyl levulinate; PrL: propyl levulinate.

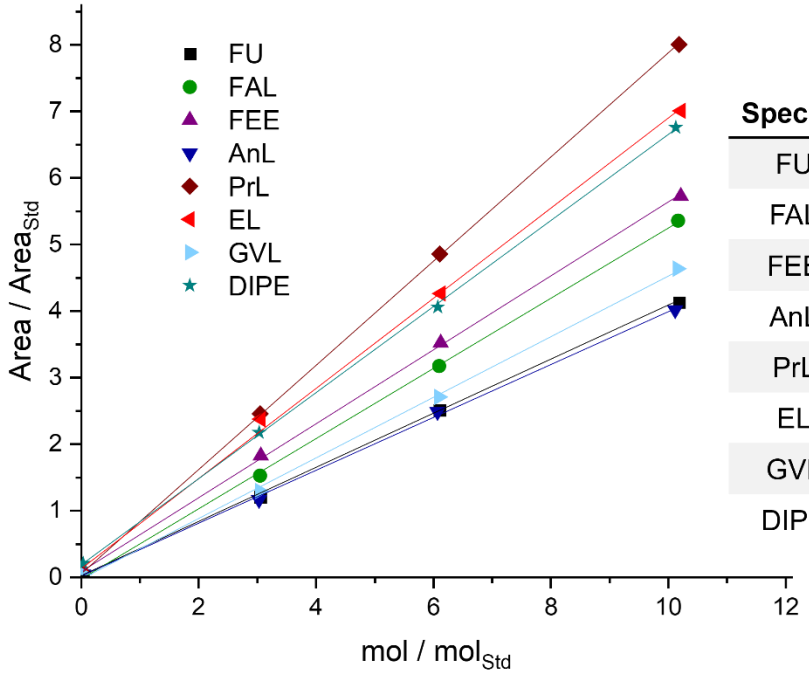

Species	RF
FU	0.405
FAL	0.519
FEE	0.562
AnL	0.395
PrL	0.785
EL	0.689
GVL	0.447
DIPE	0.666

Figure S5. Calibration curves of the commercial standards utilized for the quantification of the reaction products. In the table, the response factors of each standard.

Furfuryl isopropyl ether (FPE) and isopropyl levulinate (IPL) are not commercially available. To calculate their selectivity their response factor was assumed to be that of the most similar commercially available substitute. For FPE, furfuryl ethyl ether (FEE) was employed, while for IPL, n-propyl levulinate (PrL) was chosen.
The post reaction solutions were analysed via GC, then the molar amount of each species was calculated as follows:

$$n_i = \frac{A_i}{A_{Std}} * \frac{n_{Std}}{RF_i}$$

Conversion of the substrate was calculated as

$$X = 100 * \left(1 - \frac{n_{Sub}}{n_{Sub,t=0}}\right)$$

The selectivity of each quantified product was calculated as

$$S_i = 100 * \frac{n_i}{n_{Sub,t=0} - n_{Sub}}$$

The productivity was calculated as an average value from the beginning to the end of the batch reaction, in order to be comparable with the results obtained from the literature:

$$P_{GVL} = \frac{n_{0,FU} * X_{FU} * S_{GVL}}{m_{Cat} * t_R} = \frac{n_{0,FU} * Y_{GVL}}{m_{Cat} * t_R}$$

Results and Discussion

Entries 1-3 of **Table S1** represent Aquivion-Silica composites with varying polymer contents (40 wt%, 30 wt% and 20 wt%); entries 2, 4 and 5 represent composites with constant Aquivion content (30wt%) and varying oxide (silica, titania, zirconia); lastly, entries 5-7 represent Aquvion-Zirconia composites with varying polymer content (30 wt%, 20 wt% and 10 wt%).

Table S1. Main properties of the synthesized catalysts and the employed oxides.

Entry	Catalyst	Polymer content (wt%)[a]	BET SSA[b] ($m^2\ g^{-1}$)	V_{Pores}[b,c] ($cm^3\ g^{-1}$)	D_{Avg}[b,d] (nm)
1	Aq/SiO_2 40%	43	34	0.12	13.8
2	Aq/SiO_2 30%	29	75	0.17	9.0
3	Aq/SiO_2 20%	18	116	0.21	7.3
4	Aq/TiO_2 30%	32	23	0.21	35
5	Aq/ZrO_2 30%	28	116	0.15	4.8
6	Aq/ZrO_2 20%	21	140	0.15	4.4
7	Aq/ZrO_2 10%	10	209	0.21	4.2
8	SiO_2	-	188	0.35	5.9
9	TiO_2	-	80	0.19	15
10	ZrO_2	-	250	0.28	4.5

[a] Measured via TGA; [b] Measured via N_2 adsorption/desorption porosimetry; [c] Total pores volume; [d] Average pore diameter.

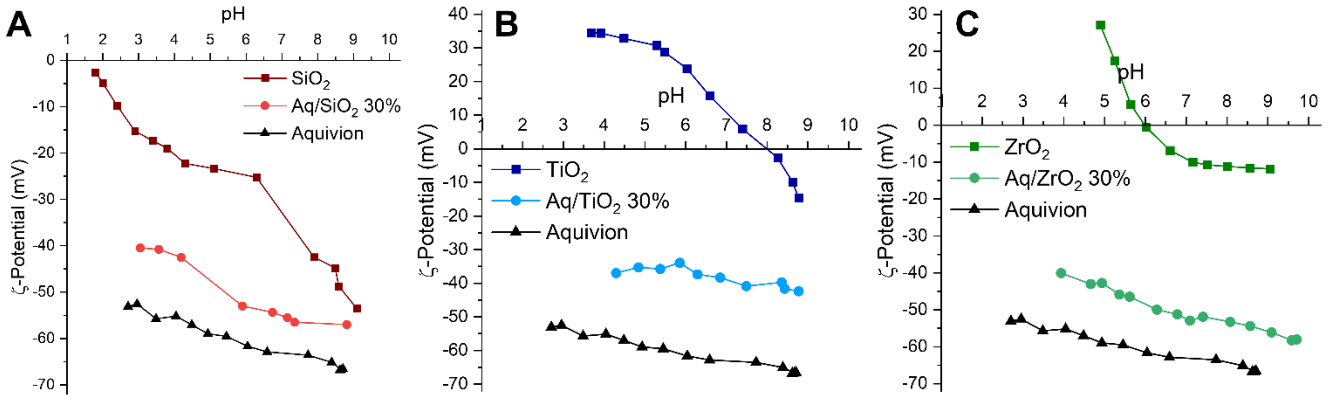

Figure S6. Influence of pH on the ζ-potential of the suspensions employed for the spray-freeze drying.

To properly understand the properties of Aquivion/Oxide SFD composite materials, the use of silica enables the study of the behaviour of Aquivion within these composites in absence of a Lewis acid component. For this reason, a series of Aquivion/Silica composites with different polymer contents in the 20-40wt% range were prepared (entries 1-3 of **Table S1**).

SUPPORTING INFORMATION

Aquivion/Silica composites

Characterisation

Characterisation of these materials by SEM analysis showed that the presence of a granular structure (figure S7), with an open cells foam structure that characterises the two composites with the lower polymer content.

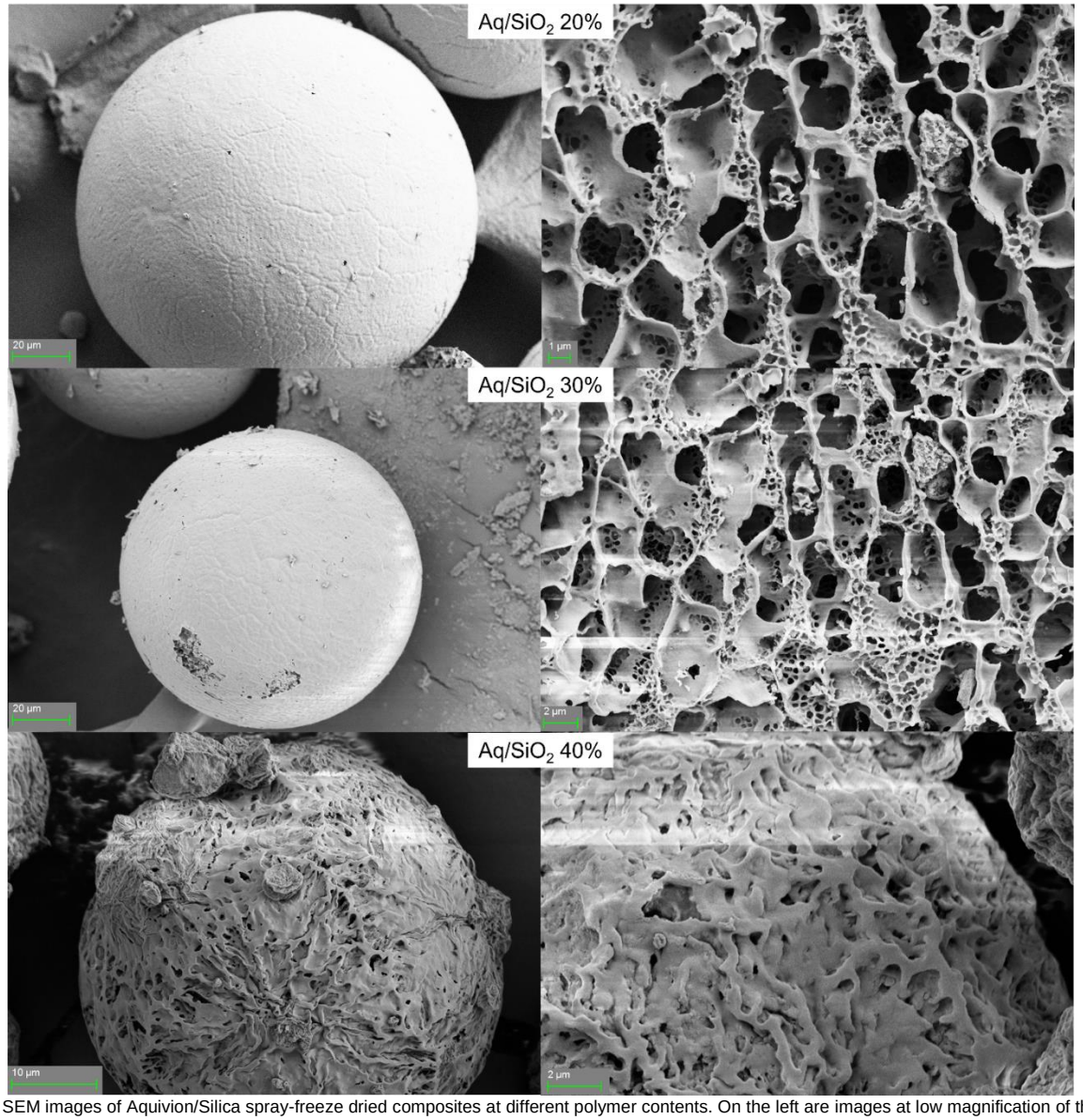

Figure S7. SEM images of Aquivion/Silica spray-freeze dried composites at different polymer contents. On the left are images at low magnification of the granular structure, while on the right are images at higher magnification to show the finer structure.

N_2 adsorption/desorption porosimetry (Figure S8) revealed type IV isotherms, characteristic of mesoporous materials, as well as the specific surface areas reported in Table S1

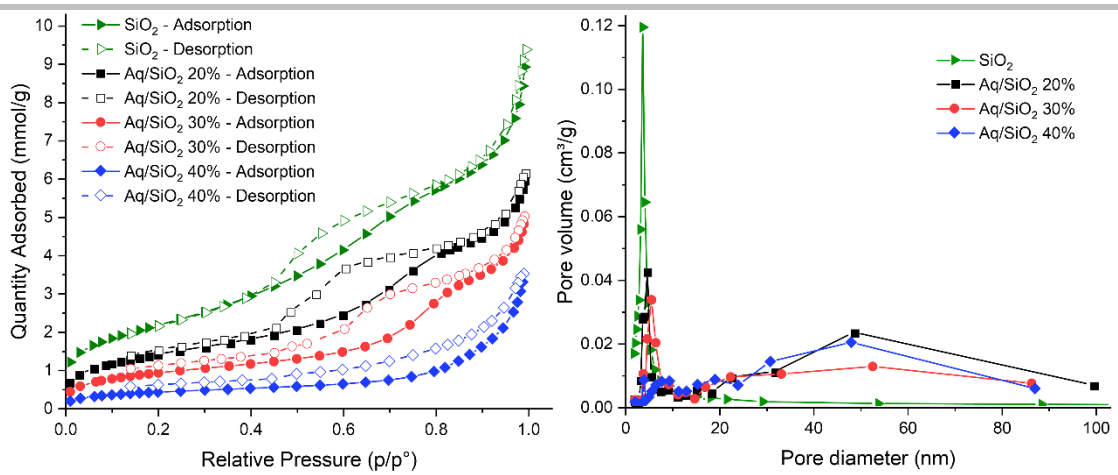

Figure S8. N_2 adsorption/desorption isothermal profiles (left) and pore size distribution (right) of Aquivion-Silica spray-freeze dried composites with different polymer contents.

TG analysis (Figure S9) shows the expected decomposition profiles of Aquivion[2], and the ratio between the weight loss in the 200-700 °C range and the weight at 200 °C revealed a polymer content very similar to the expected value (18%, 29% and 43% compared to the expected values of 20%, 30% and 40%)

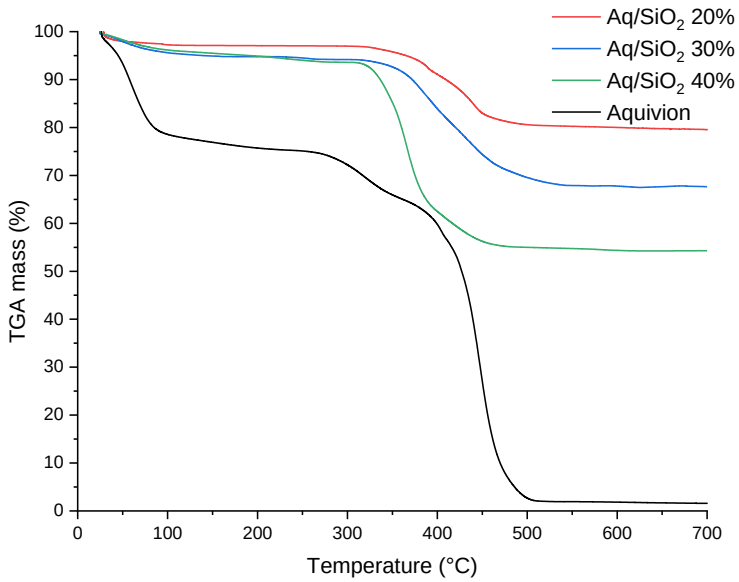

Figure S9. TGA profiles of the Aquivion-Silica spray-freeze dried composites with different polymer contents (wt%).

Catalytic testing

Blank tests (Figure S10) confirm that, in the absence of a catalyst, the reaction does not proceed in any significant manner, only leading to a small amount of etherification of FAL with the solvent, yielding FPE.

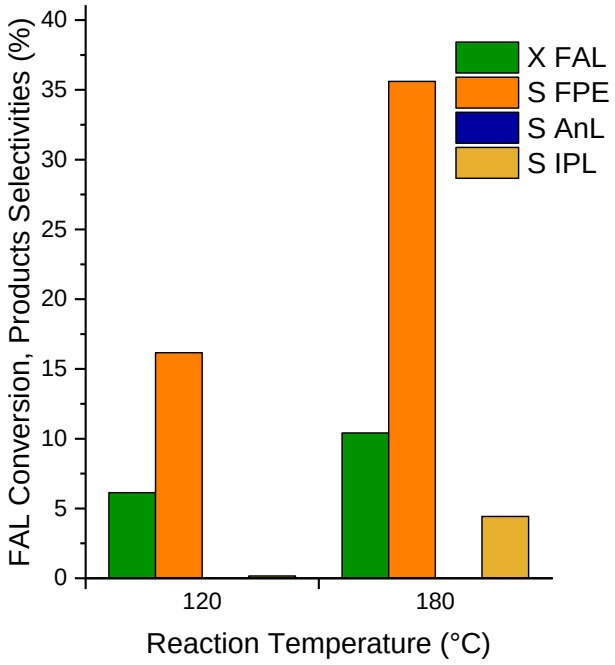

Figure S10. Blank tests at two different reaction temperatures. Reaction conditions: 1 mmol of FAL; 15 mL of isopropanol; N_2 pressure of 10 bar; Reaction time of 2 h.

These materials were tested as catalysts for the conversion of furfuryl alcohol to isopropyl levulinate and compared with the catalytic performance of pure Aquivion, (Figure S11). This reaction was chosen as a relevant part of the whole cascade process. While the conversion of FU to FAL and of isopropyl levulinate (IPL) to GVL are CTH reactions and require LAS, the steps required for the conversion of FAL to IPL are BAS-promoted, and can be catalysed by Aquivion.[3] The first and main product is furfuryl isopropyl ether (FPE), which derives from the etherification of FAL with the solvent. From the rearrangement of FAL, angelica lactones (AnL) can be produced in both the α and β isomers. Lastly, the final product of this BAS-promoted reaction is isopropyl levulinate (IPL), obtained either via transesterification of AnL or via hydrolytic ring opening of FPE. The catalytic results show that, while all these materials are active in the conversion of FAL, with only marginal differences in its conversion rate, the product distribution differs significantly. Among the tested materials, Aq/SiO_2 30% showed the highest selectivity towards IPL (35%), as well as the highest carbon balance (87%). In particular, the higher AnL selectivity (8%) coupled with a slightly lower conversion (95%) might suggest a less prominent swelling of the polymer in this catalyst, which could lead to a lower retention of the molecules of interest on the surface of the catalyst. Conversely, pure Aquivion showed the lowest carbon balance in the series (62%); furthermore, the swelling of the pure polymer led to a highly adhesive gel phase and proved difficult to recover at the end of the reaction.

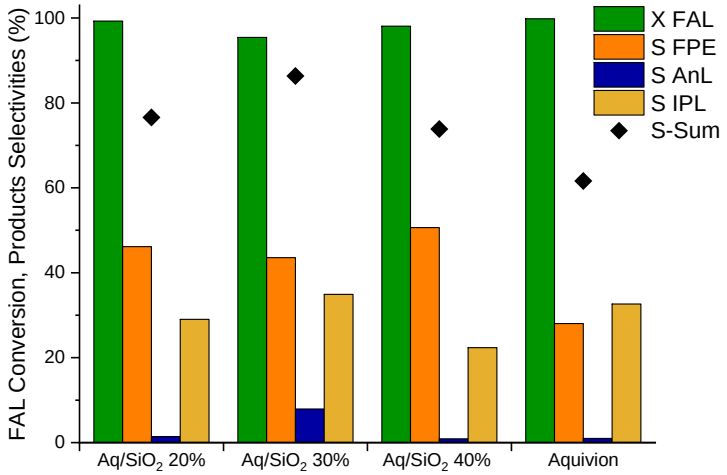

Figure S11. Effect of the polymer content within Aquivion-Silica spray-freeze dried composite catalysts and pure Aquivion. S-Sum: Sum of the selectivity of all the products of interest. Reaction conditions: 1 mmol of FAL; FAL/BAS = 100 mol/mol; 15 mL of isopropanol; N_2 pressure of 10 bar; Reaction temperature of 120 °C; Reaction time of 2 h.

Having identified Aq/SiO_2 30% as the most promising catalyst in the series, further studies were carried out to investigate the influence of the different reaction parameters and therefore to better understand the reaction mechanism. Figure S12 represents the effect of reaction time at 120 °C. From the evolution of selectivities as a function of reaction time it can be observed that at this reaction temperature the conversion of FAL reached 95% after 2h, while FPE selectivity remained almost constant in the range of 40-45%. This suggests that at this temperature the hydrolytic ring opening required to convert FPE to IPL is not effectively promoted by the catalyst.

Most notably, even at low reaction times, there was more than 10% selectivity towards IPL, which only increased up to 45% despite the inability to convert FPE. This was attributed to the conversion of FAL to 4,5,5-triisopropoxypentanone (TIPP), which can be converted to IPL, but is not a stable compound and can't be reliably quantified via gas chromatography.[4,5]

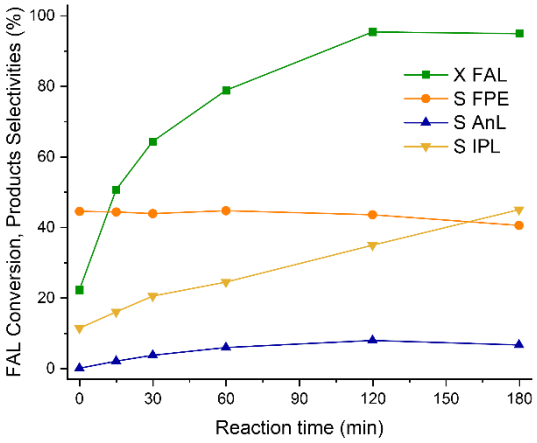

Figure S12. Effect of reaction time on the catalytic performances of Aq/SiO_2 30% at 150 °C. Reaction conditions: 1 mmol of FAL; FAL/BAS = 100 mol/mol; 15 mL of isopropanol; N_2 pressure of 10 bar.

Similar studies on the effect of reaction time were also carried out at different reaction temperatures, for example at 150 °C (Figure S13) and 180 °C (Figure S14), showing that FPE can be converted to IPL at 150 °C, and that these catalysts are unable to convert AnL to IPL even at 180°C. Comparing instead the selectivities obtained varying the reaction temperature at a constant reaction time of 2h (Figure S15), AnL showed a very linear and constant increase in selectivity with reaction temperature. This has been correlated with the diisopropyl ether production via etherification of two molecules of the solvent, (Figure S16). This process releases a molecule of water, thus suggesting the fact that product selectivity can be influenced by the quantity of water present in the reaction system, which changes with reaction temperature due to a different degree of dehydration of the solvent. To further investigate this aspect, a study was carried out adding to the reaction system either 1 mmol of sodium sulphate anhydrous as a water-sequestering agent or a variable amount of water (0.5-3 mmol, Figure S17). The results reported in Figure S17 showed that sodium sulphate inhibited both the conversion of FPE and the formation of AnL. On the contrary, the addition of water improved the catalytic performances up to 1mmol (H_2O/FAL molar ratio of 1), leading to an IPL selectivity of 81% and a 97% carbon balance. This was explained with the fact that the main process through which carbon balance was lowered in these reactions, the formation of humins from FAL, started with the etherification of two molecules of FAL to produce difurfuryl ether (DFE); this reaction is an equilibrium that releases water, hence the addition of water to the system inhibits it.

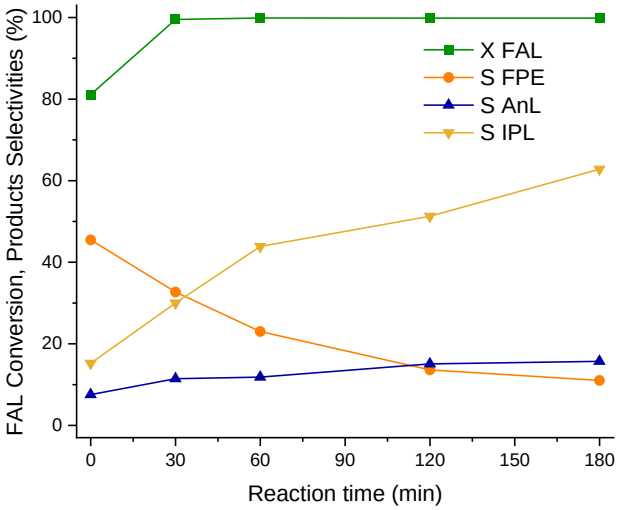

Figure S13. Effect of reaction time on the catalytic performances of Aq/SiO_2 30% at 150 °C. Reaction conditions: 1 mmol of FAL; FAL/BAS = 100 mol/mol; 15 mL of isopropanol; N_2 pressure of 10 bar.

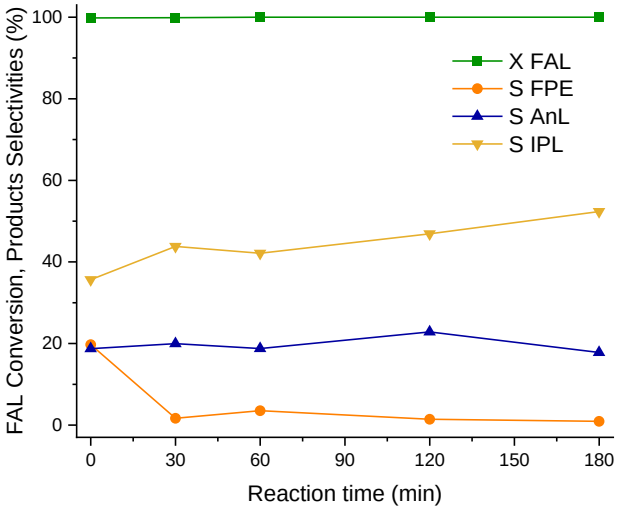

Figure S14. Effect of reaction time on the catalytic performances of Aq/SiO_2 30% at 180°C. Reaction conditions: 1 mmol of FAL; FAL/BAS = 100 mol/mol; 15 mL of isopropanol; N_2 pressure of 10 bar.

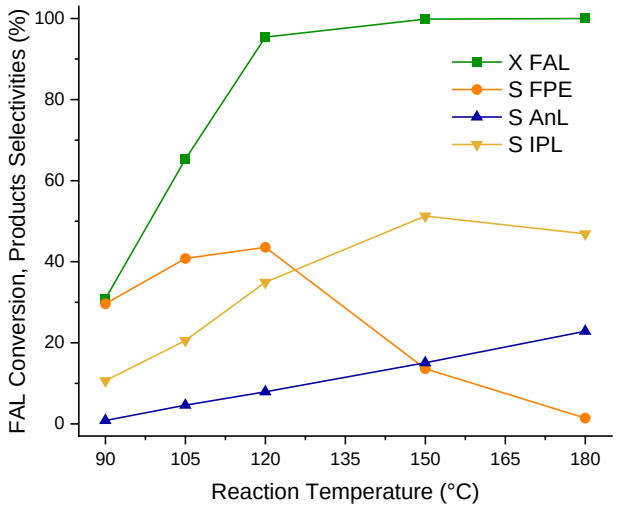

Figure S15. Effect of reaction temperature on the catalytic performances of Aq/SiO_2 30%. Reaction conditions: 1 mmol of FAL; FAL/BAS = 100 mol/mol; 15 mL of isopropanol; N_2 pressure of 10 bar; Reaction time of 2 h.

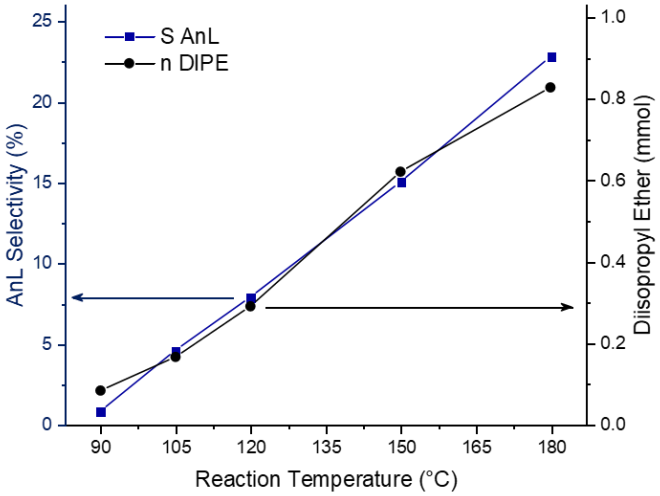

Figure S16. Effect of reaction temperature on the production of diisopropyl ether with Aq/SiO_2 30%. Reaction conditions: 1 mmol of FAL; FAL/BAS = 100 mol/mol; 15 mL of isopropanol; N_2 pressure of 10 bar; Reaction time of 2 h.

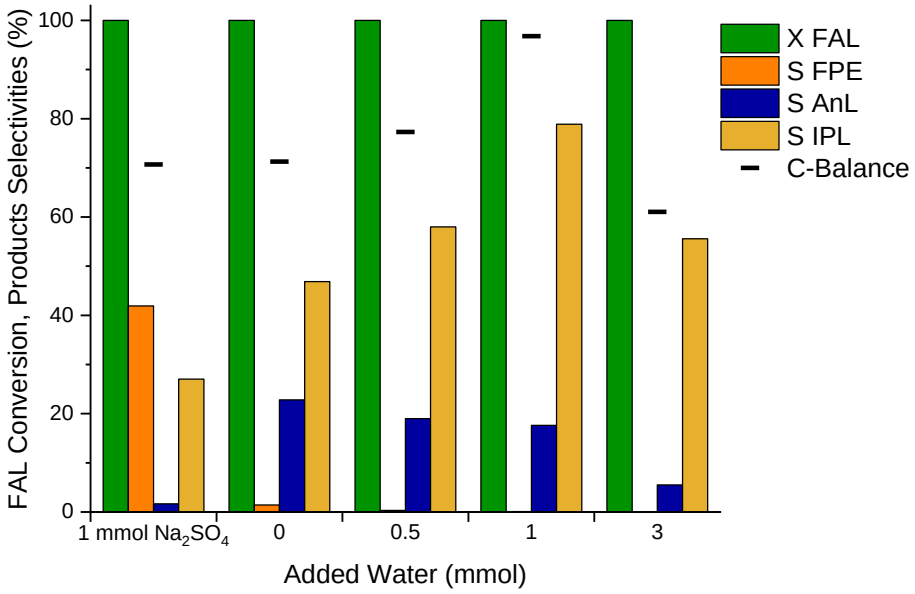

Figure S17. Effect of the water content on FAL conversion in the presence of Aq/SiO_2 30% catalyst. Reaction conditions: 1 mmol of FAL; FAL/BAS = 100 mol/mol; 15 mL of isopropanol; N_2 pressure of 10 bar; Reaction temperature of 180 °C; Reaction time of 2 h. Compared to the standard reaction (marked as 0 mmol of added water), either 1 mmol of anhydrous Na_2SO_4 (on the left) or 0.5-1-3 mmol of water (on the right) were added.

A new study on the effect of reaction temperature was carried out in presence of 1mmol of water (Figure S18), highlighting an overall better catalytic performance, especially regarding the degradation of the species of interest, which is inhibited by the presence of water, as represented in Figure S19.

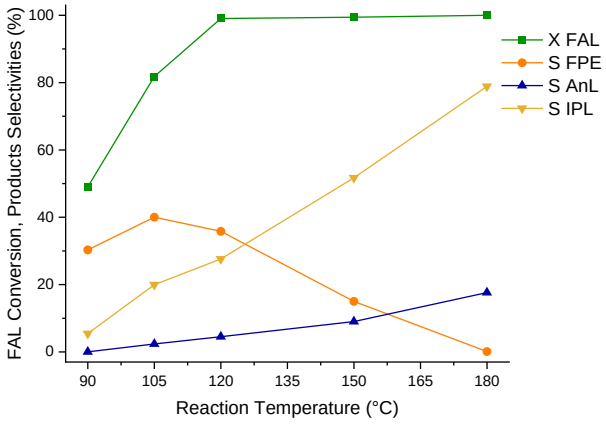

Figure S18. Effect of reaction temperature on the catalytic performances of Aq/SiO_2 30% in presence of 1eq of water. Reaction conditions: 1 mmol of FAL; FAL/BAS = 100 mol/mol; 1eq of water; 15 mL of isopropanol; N_2 pressure of 10 bar; Reaction time of 2 h.

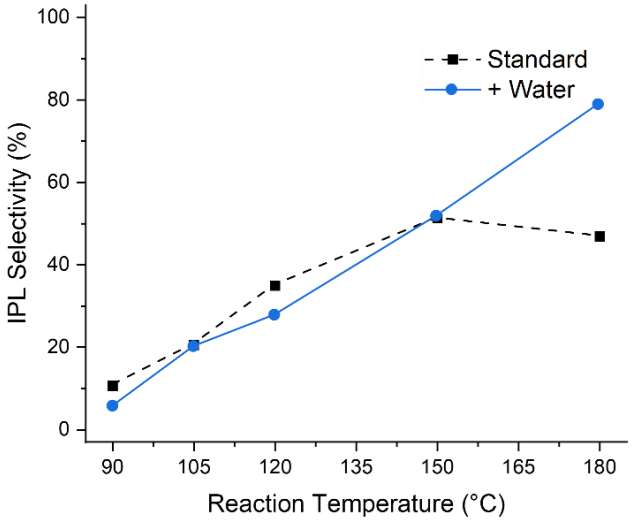

Figure S19. Comparison between the IPL selectivity at different temperature over Aq/SiO_2 30% in presence and in absence of added water. Reaction conditions: 1 mmol of FAL; FAL/BAS = 100 mol/mol; 0 or 1eq of water (Standard and +Water curves, respectively); 15 mL of isopropanol; N_2 pressure of 10 bar; Reaction time of 2 h.

To ensure the significance of the results, the default stirring rate (600 rpm) in the reaction vessel was changed to ensure mixing is not a limiting factor in the catalytic behaviour, Figure S20.

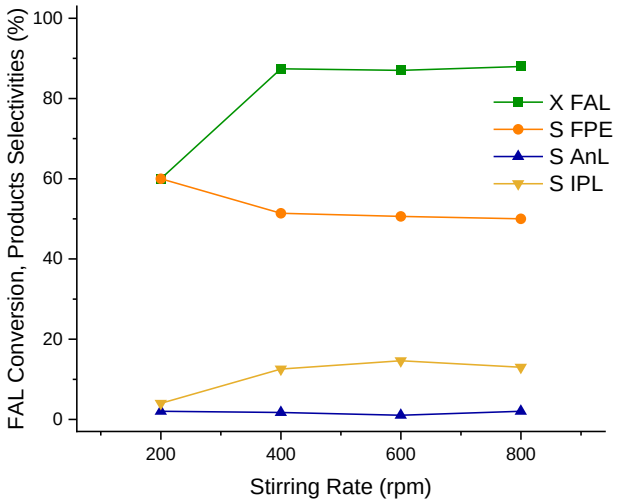

Figure S20. Effect of stirring rate on the catalytic performance of Aq/SiO_2 30%. Reaction conditions: 1 mmol of FAL; FAL/BAS = 100 mol/mol; 1 eq of water; 15 mL of isopropanol; N_2 pressure of 10 bar; Reaction temperature of 120 °C; Reaction time of 0.5 h.

To further verify that the catalyst activity is the main factor in determining the reaction outcome, isoconversion tests were carried out changing the catalyst amount (0.5% molar and 1.5% molar, compared to the standard 1% used in most of this paper) and adjusting the reaction time to achieve similar conversions. The results reported in Figure S21 show a very consistent reaction outcome, verifying the hypothesis.

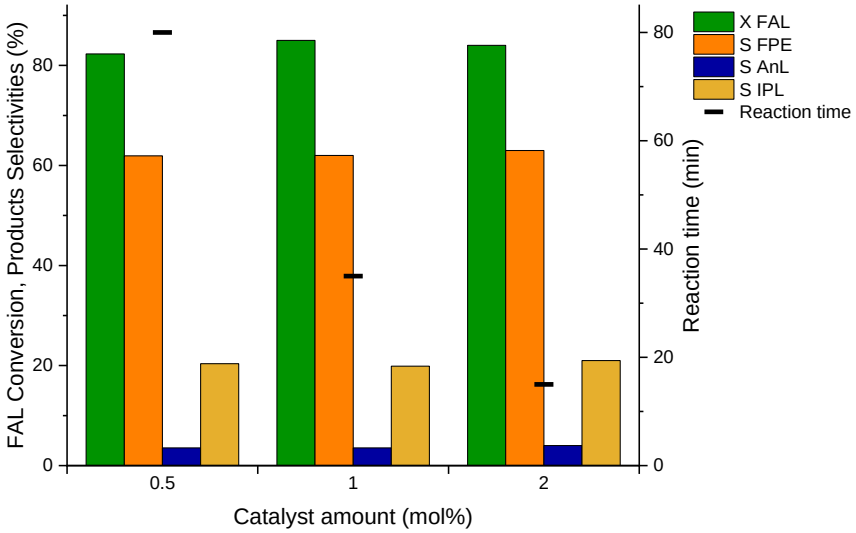

Figure S21. Isoconversion tests carried out on Aq/SiO_2 30%, varying the reaction time to achieve roughly 80% conversion. Reaction conditions: 1 mmol of FAL; FAL/BAS = 200 (left), 100 (middle) or 50 (right) mol/mol; 1eq of water; 15 mL of isopropanol; N_2 pressure of 10 bar; Reaction temperature 120 °C.

Study on the effect of the metal oxide within Aquivion-based composites

Characterisation

In order to introduce Lewis acidity in the composites, the synthesis of high surface area zirconia to be employed in the synthesis of the composites was tuned. In particular, the effect of calcination temperature was investigated. From the XRD patterns in Figure S22, it can be observed that there is an increase in crystallinity after calcination at 550 °C or more. This is undesirable, given that it is accompanied by a decrease in surface area (Figure S23) and acid sites density (Figure S24), as well as catalytic activity (Figure S25)

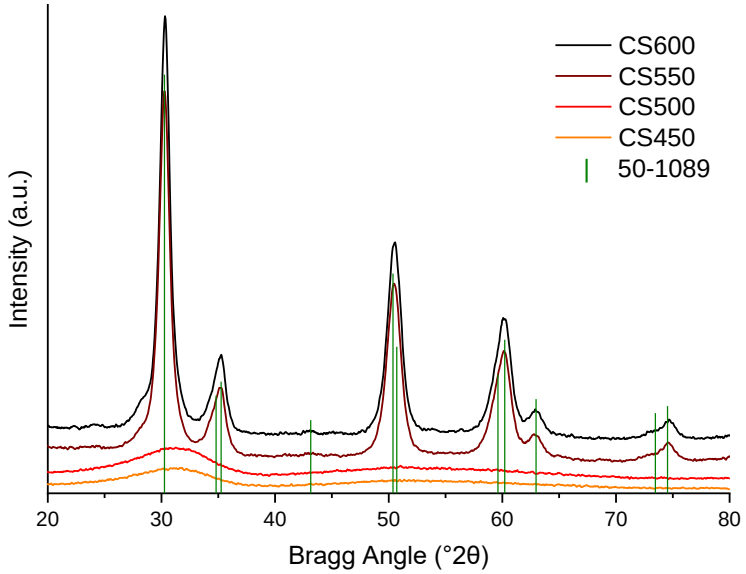

Figure S22. XRD patterns of the synthesized zirconia calcined at different temperatures. “CSXXX” stands for “Calcined in Static air at XXX °C”. In green, the reference pattern of tetragonal zirconia from PDF 50-1089.

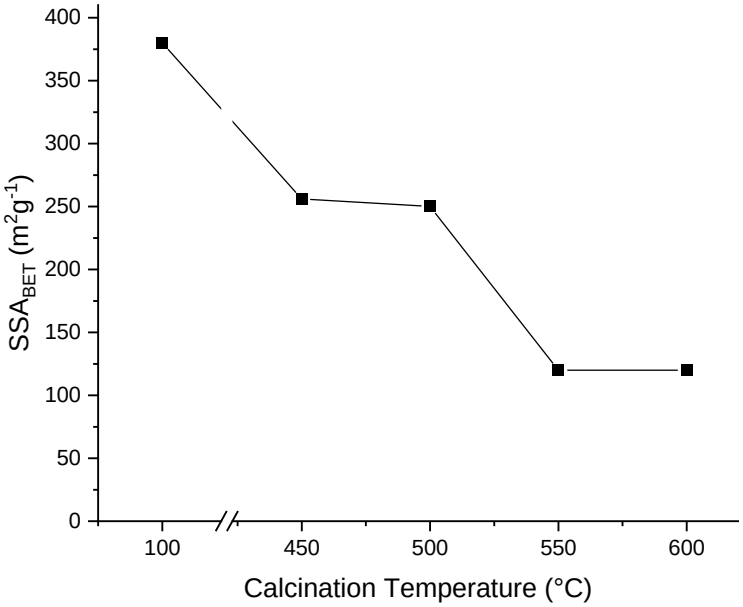

Figure S23. Effect of the calcination temperature on the BET Specific Surface Area of the synthesized zirconia.

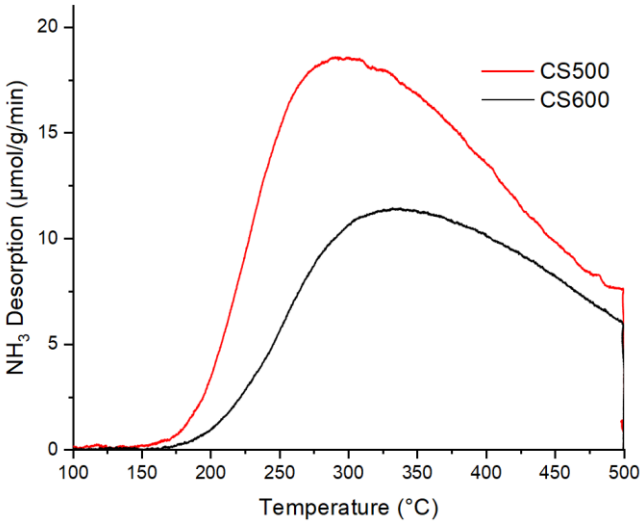

Figure S24. NH_3 temperature-programmed desorption profile for ZrO_2 calcined at 500 °C (CS500) and 600 °C (CS600).

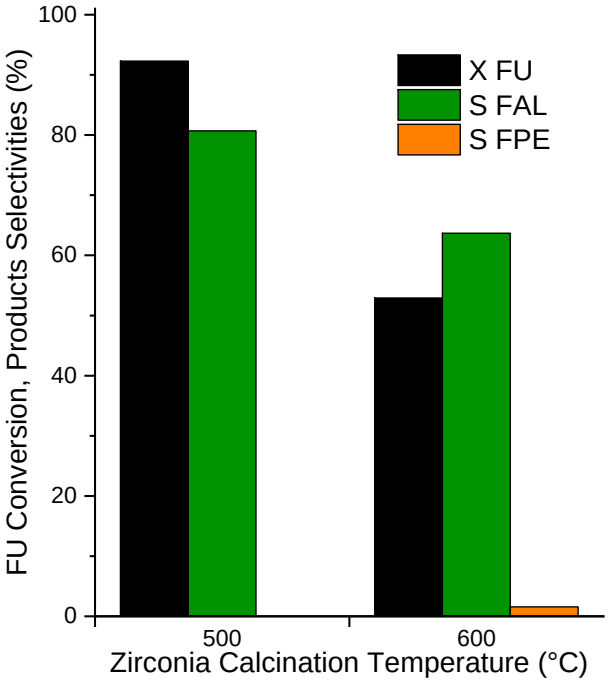

Figure S25. Effect of calcination temperature on the performance of high surface area tetragonal zirconia in the CTH of furfural. Reaction conditions: 1 mmol of FU; FU/Lewis acid sites = 80 mol/mol (25 mg of catalyst); 1 eq of water; 15 mL of isopropanol; N_2 pressure of 10 bar; Reaction time of 1 h; Reaction temperature of 180 °C.

NH_3-TPD (Figure S26) reveals a different amount of acid sites in the three oxides employed.

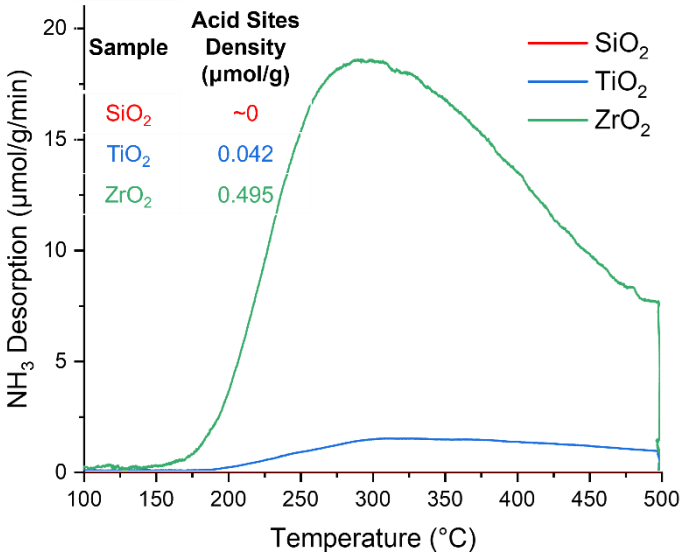

Figure S26. NH_3 temperature-programmed desorption profile for SiO_2, TiO_2, and ZrO_2 calcined at 500 °C.

Despite their very different specific surface area, all the composites show microporous structure upon inspection with N2 adsorption/desorption porosimetry (Figure S27). ζ-potential measurements (Figure S28) suggest a matrix encapsulation structure, due to the similarity between the behaviour of the mixed suspension with that of pure Aquivion.

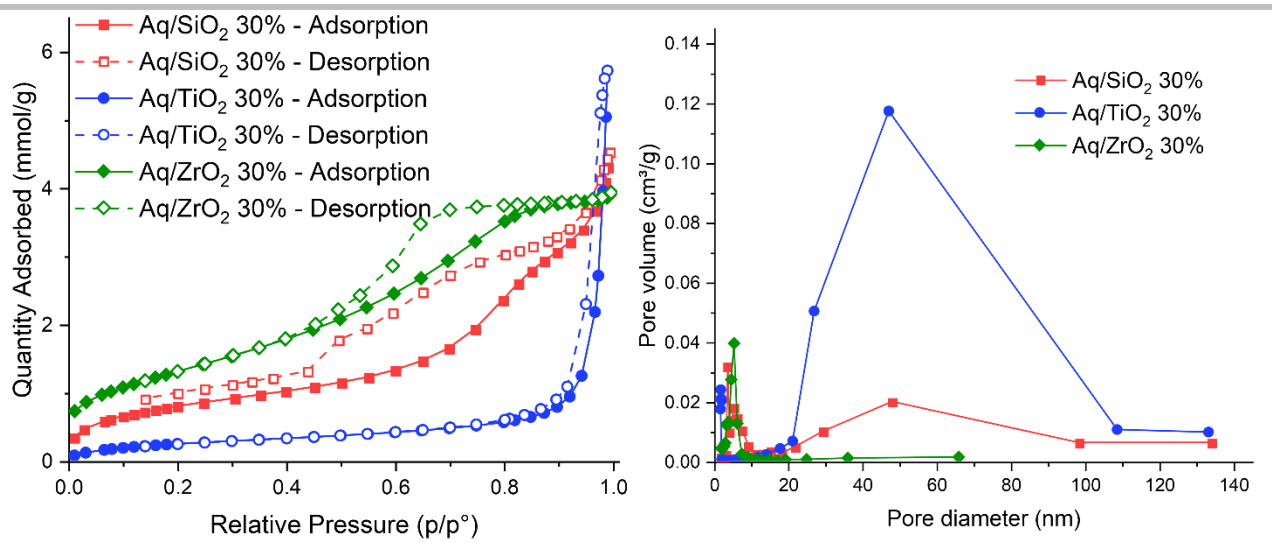

Figure S27. N_2 adsorption/desorption isothermal profiles (left) and pore size distribution (right) of Aquivion-based spray-freeze dried composites with different oxides.

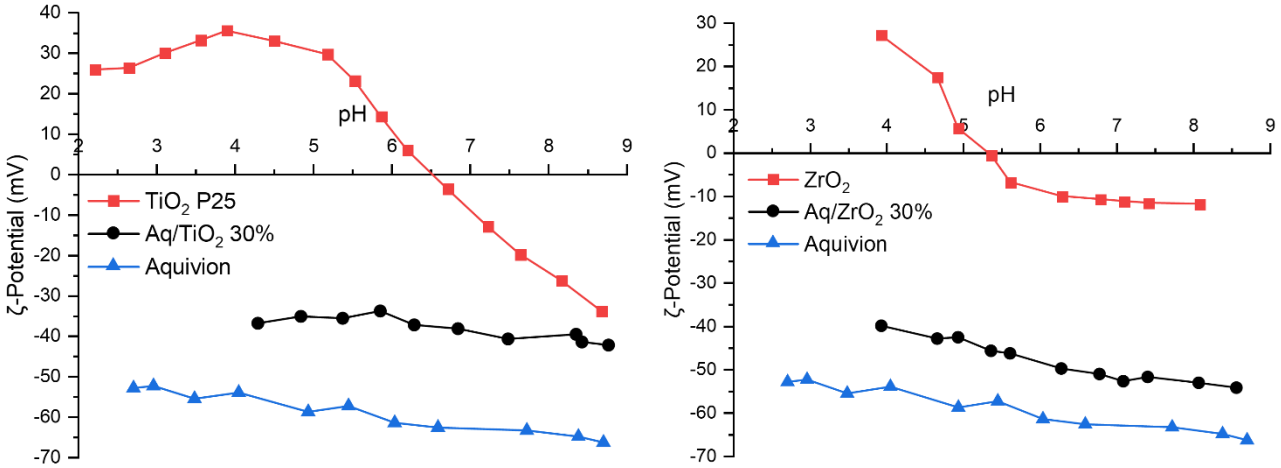

Figure S28. Influence of pH on the ζ-potential of Aquivion, titania and zirconia-based suspensions.

TGA profiles (Figure S29) once again reveal a reliable polymer content, varying from 28% to 32% against the theoretical 30%.

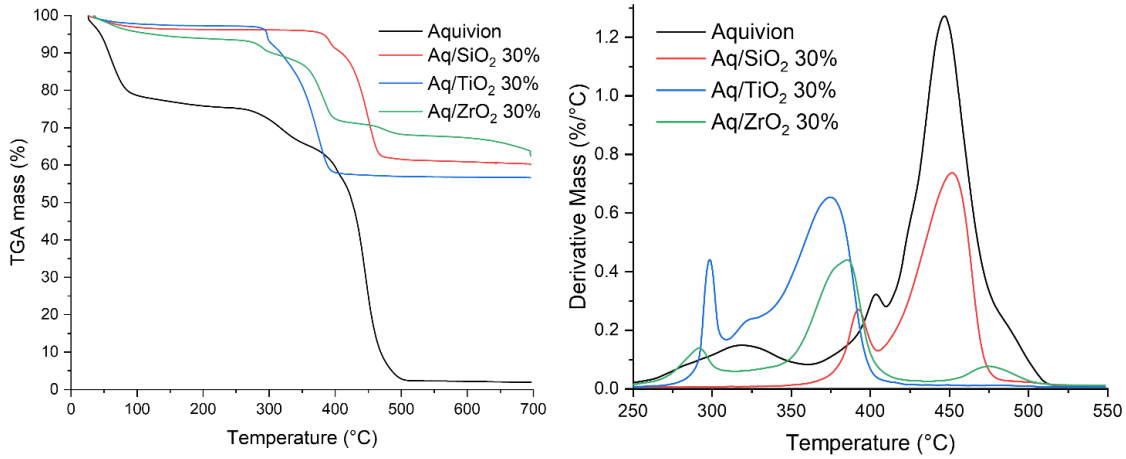

Figure S29. TGA (left) and DTG (right) profiles of Aquivion and Aquivion-based spray-freeze dried composites with varying oxide.

SEM imaging showed that the presence of a granular structure (Figure S30 and Figure S31) with good superimposability of the EDX maps of the fluorine and the metal of the oxide (Ti or Zr, Figure S32 and Figure S33)

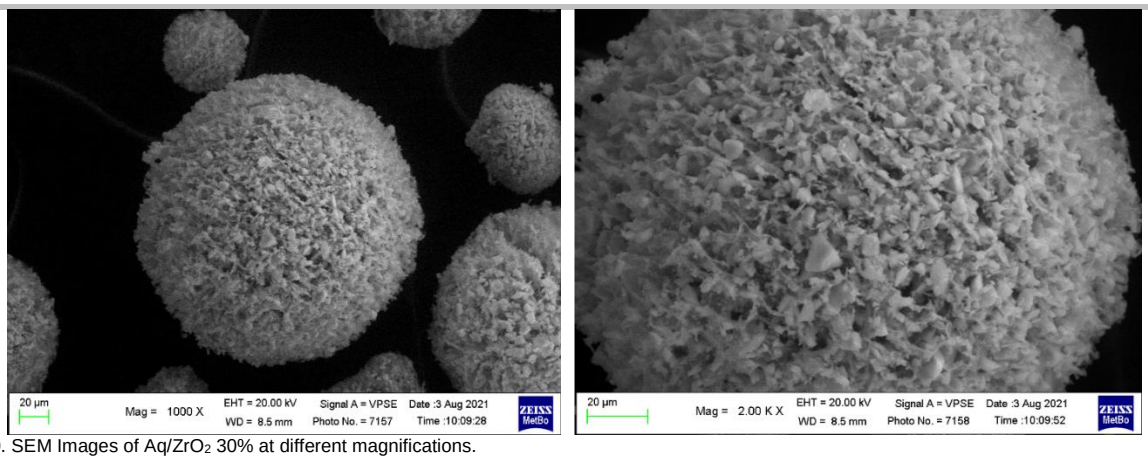

Figure S30. SEM Images of Aq/ZrO_2 30% at different magnifications.

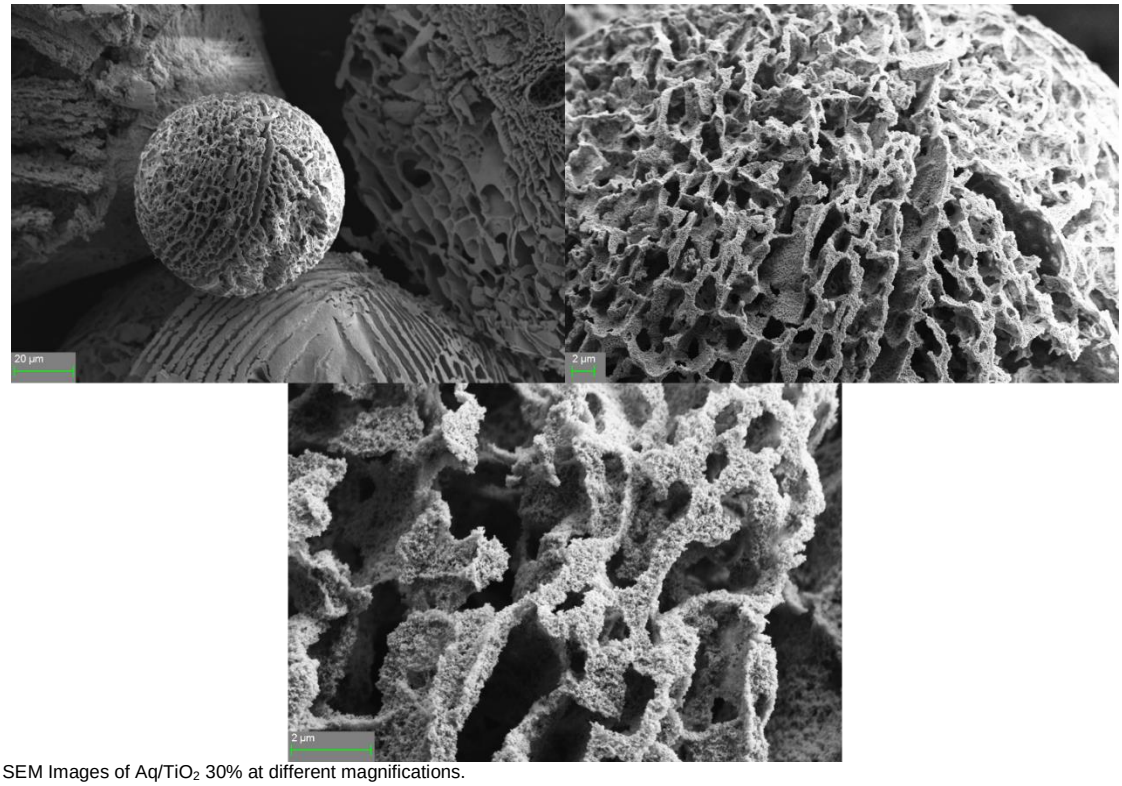

Figure S31. SEM Images of Aq/TiO_2 30% at different magnifications.

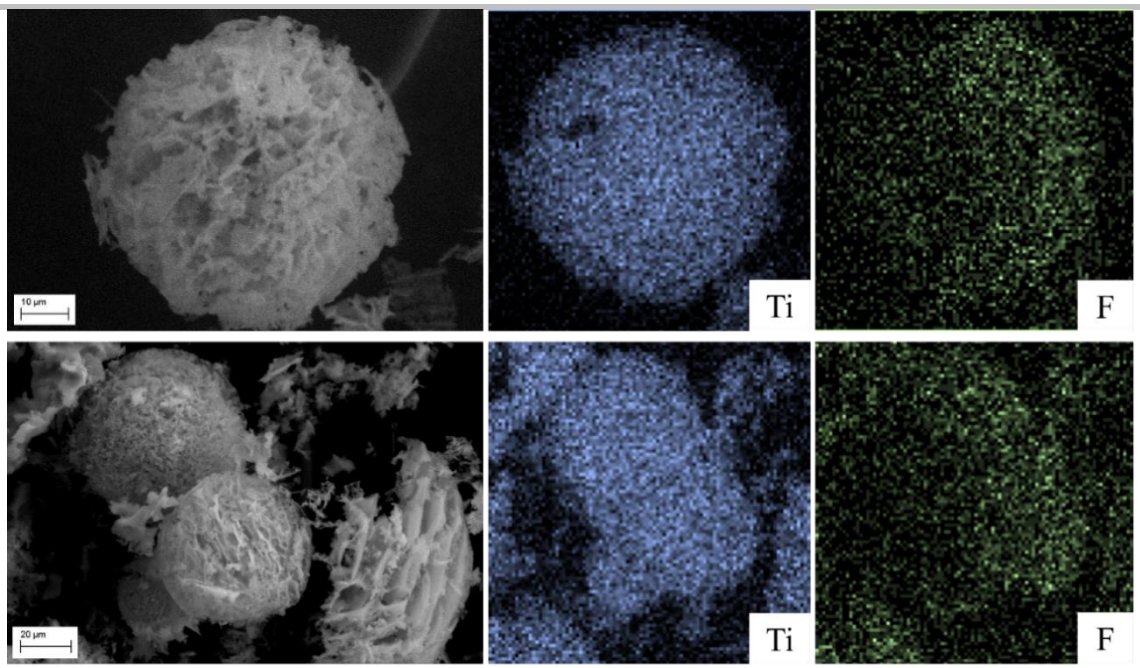

Figure S32. SEM Imaging and SEM-EDX mapping of Ti and F for Aq/TiO_2 30% (above) and Aq/TiO_2 30% calcined at 200 °C (below).

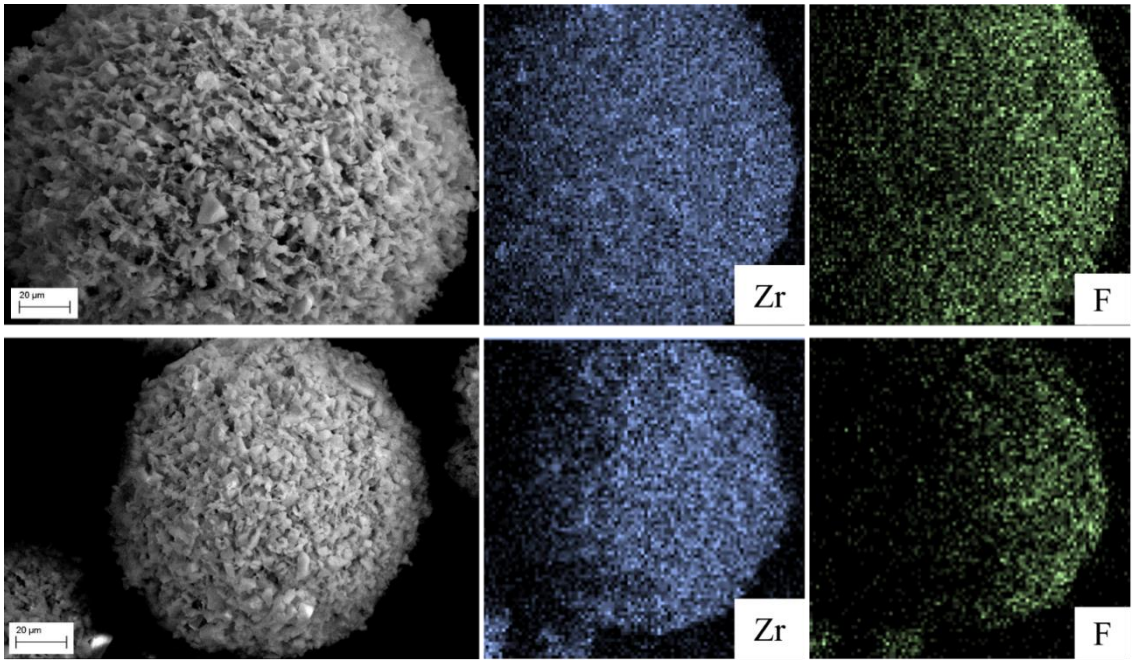

Figure S33. SEM Imaging and SEM-EDX mapping of Zr and F for Aq/ZrO_2 30% (above) and Aq/ZrO_2 30% calcined at 200 °C (below).

TEM imaging (Figure S34) confirms the matrix encapsulation suggested by the ζ-potential measurements, showing a structural role of Aquivion in holding together the granules of nanocrystalline zirconia (Figure S35).

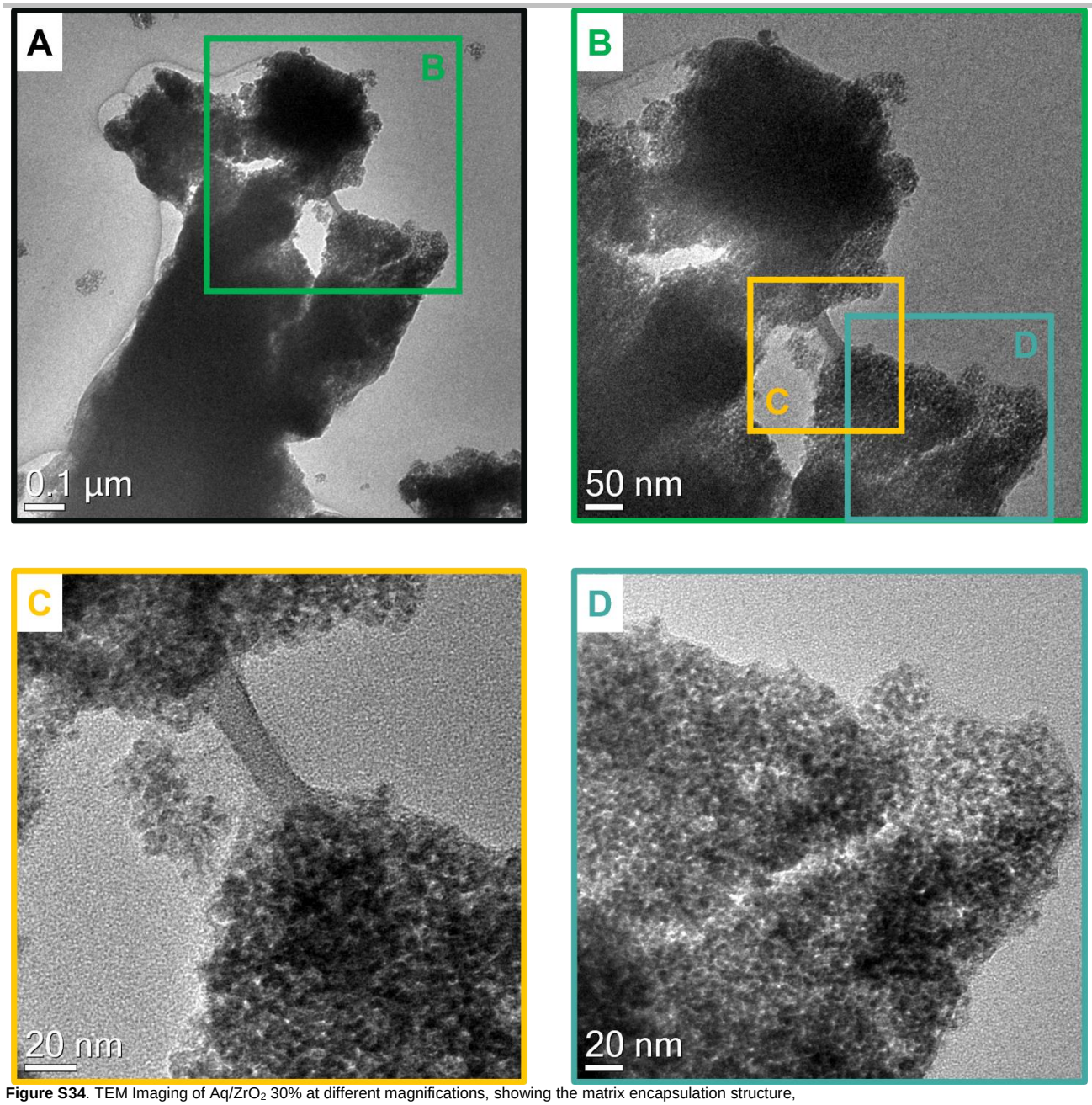

Figure S34. TEM Imaging of Aq/ZrO_2 30% at different magnifications, showing the matrix encapsulation structure,

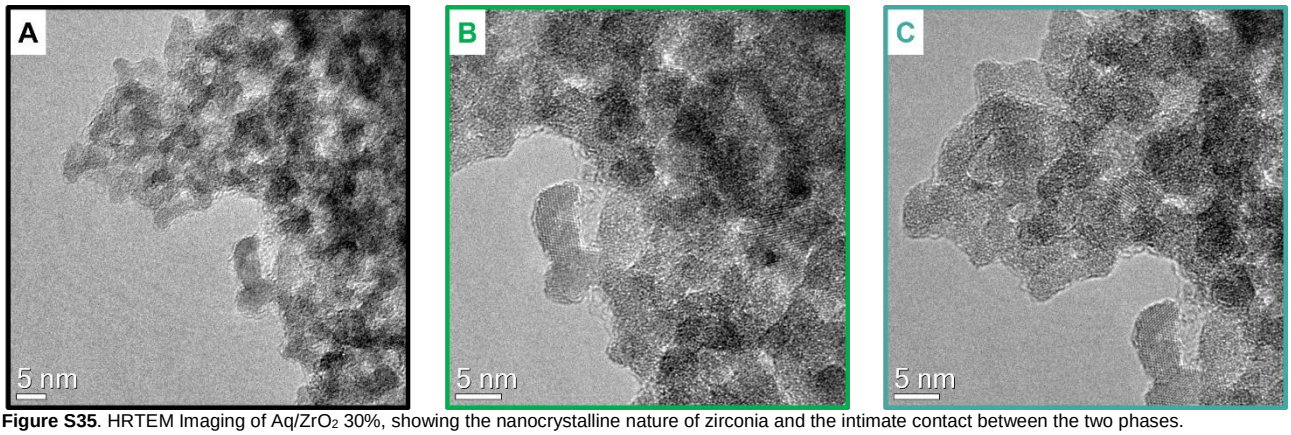

Figure S35. HRTEM Imaging of Aq/ZrO_2 30%, showing the nanocrystalline nature of zirconia and the intimate contact between the two phases.

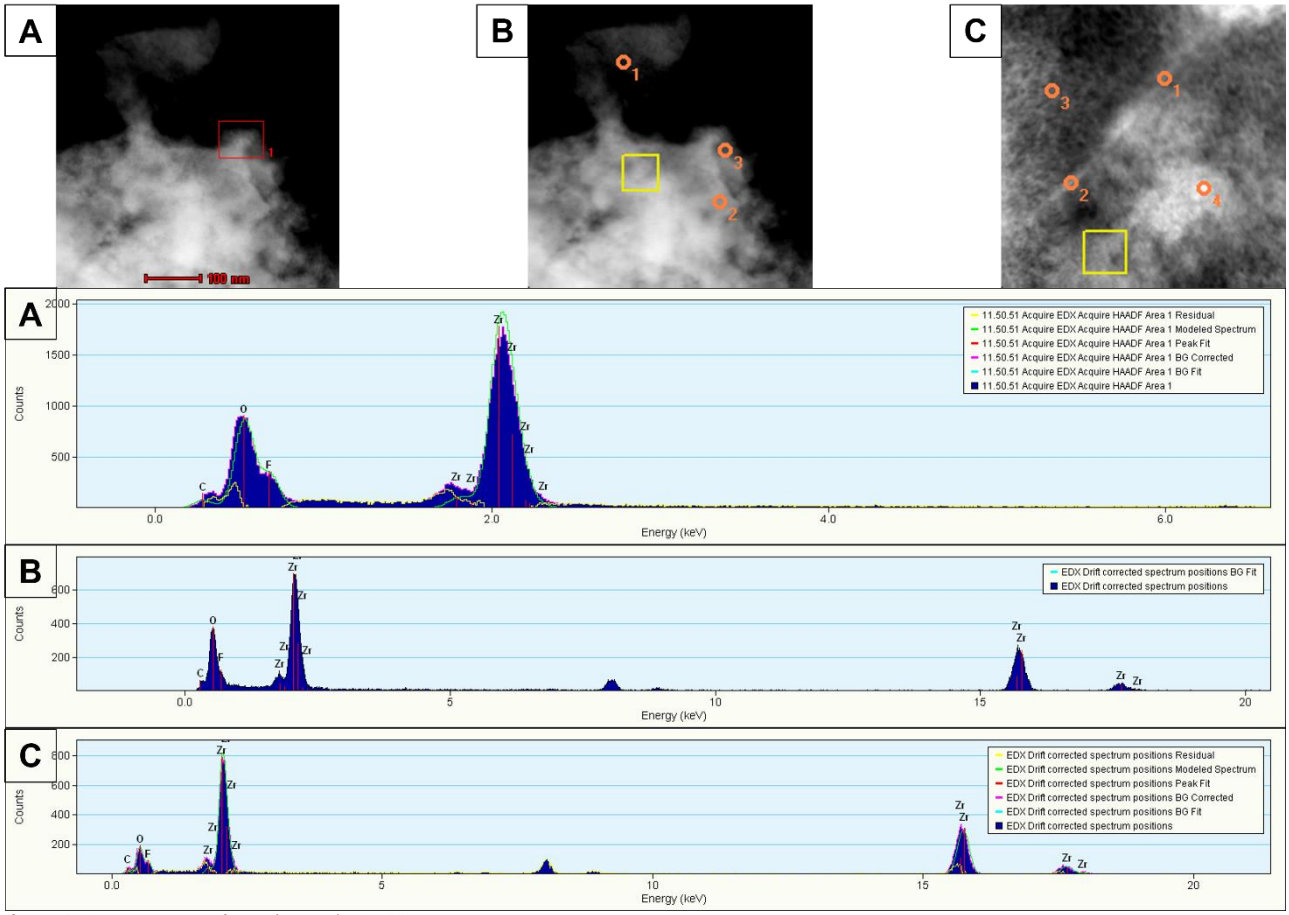

Figure S36. TEM-EDX performed on Aq/ZrO_2 30%.

Table S2. Atomic distribution of Zr, O, C and F in different morphological features of Aq/ZrO_2 30%. The samples refer to the different areas and points as marked in Figure S34.

Sample	Zr (at%)	O (at%)	C (at%)	F (at%)
Th. Avg.[a]	17.0	38.1	14.6	28.2
A-1	16.5±0.4	53.9±0.3	15.7±0.2	13.9±0.2
B-1	16.0±0.7	58.1±0.5	13.0±0.4	12.9±0.3
B-2	18.5±0.6	56.8±0.5	12.9±0.4	11.8±0.2
B-3	18.2±0.6	57.0±0.5	12.9±0.4	11.9±0.2
B-A	18.3±0.6	57.0±0.5	12.9±0.4	11.9±0.2
C-1	30.2±0.8	40.4±0.4	17.6±0.4	11.8±0.2
C-2	30.2±0.8	40.4±0.3	17.6±0.3	11.8±0.2
C-3	30.3±0.8	40.4±0.3	17.5±0.3	11.8±0.2
C-4	30.9±0.8	39.2±0.3	17.9±0.3	12.0±0.2
C-A	28.0±0.8	40.6±0.4	19.5±0.4	11.9±0.2

[a]Theoretical average atom distribution calculated from the sample's phase composition.

Catalytic testing

For Aq/TiO_2 30%, both a study on the effect of reaction temperature and the effect of reaction time at 120 °C were carried out. While the effect of reaction temperature (Figure S37) reveals selectivity profiles very similar to Aq/SiO_2 30% previously discussed, the effect of reaction time at 120 °C (Figure S38) shows that this material is capable of promoting hydrolytic ring opening of FPE at lower temperatures than the silica-based composite.

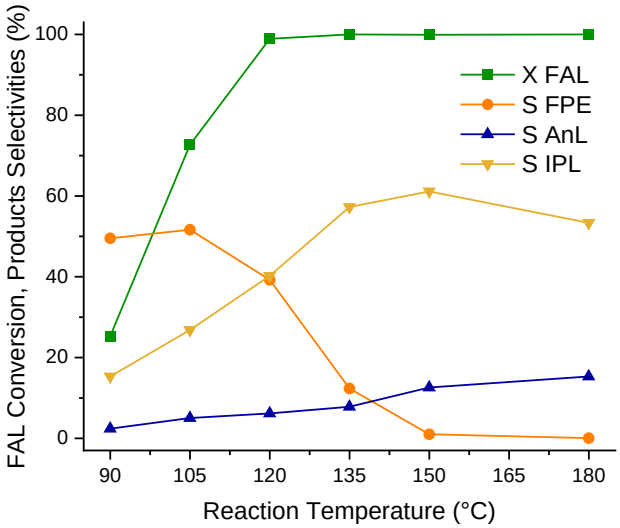

Figure S37. Effect of reaction temperature on Aq/TiO_2 30% catalytic performances. Reaction conditions: 1 mmol of FAL; FAL/BAS = 100 mol/mol; 1 eq of water; 15 mL of isopropanol; N2 pressure of 10 bar; Reaction time of 2 h.

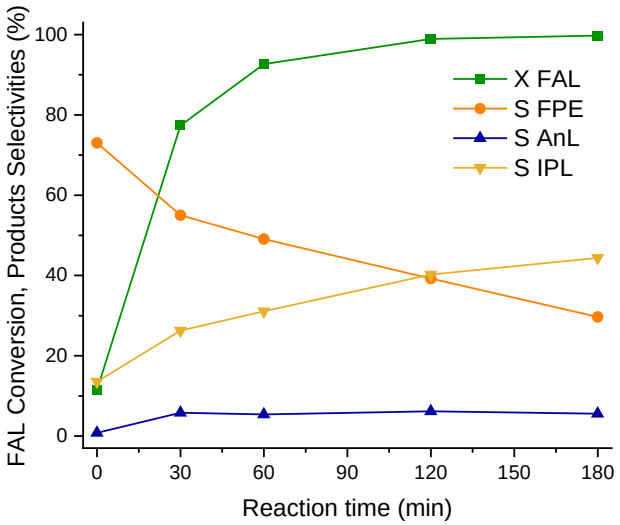

Figure S38. Effect of reaction time on Aq/TiO_2 30% catalytic performances at 120 °C. Reaction conditions: 1 mmol of FAL; FAL/BAS = 100 mol/mol; 1 eq of water; 15 mL of isopropanol; N2 pressure of 10 bar.

For Aq/ZrO_2 30% a more thorough study was carried out, with the effect of reaction time tested at 120 °C (Figure S39), 150 °C (Figure S40) and 180 °C (Figure S41) as well as the effect of reaction temperature at 2 h of reaction time (Figure S42). From these results, the promising improvement observed going from silica to titania is pushed even further, and at 150 °C a GVL selectivity is already observed. While 150 °C only leads to a modest selectivity towards GVL (20% even after 16 h), at 180 °C Aq/ZrO_2 30% is capable of producing significant amounts of GVL.

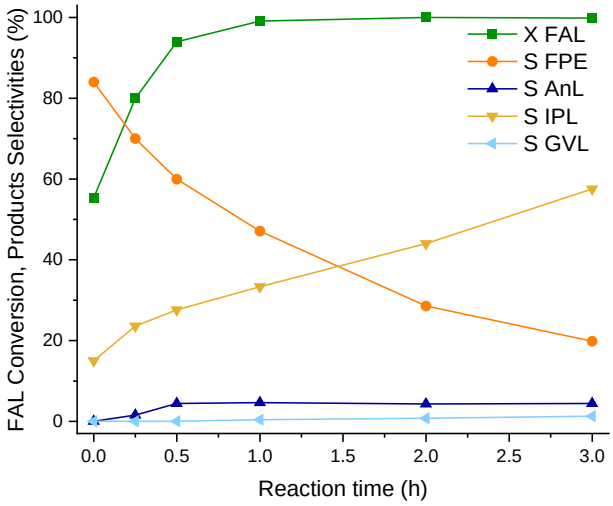

Figure S39. Effect of reaction time on Aq/ZrO_2 30% catalytic performances at 120 °C. Reaction conditions: 1 mmol of FAL; FAL/BAS = 100 mol/mol; 1 eq of water; 15 mL of isopropanol; N_2 pressure of 10 bar.

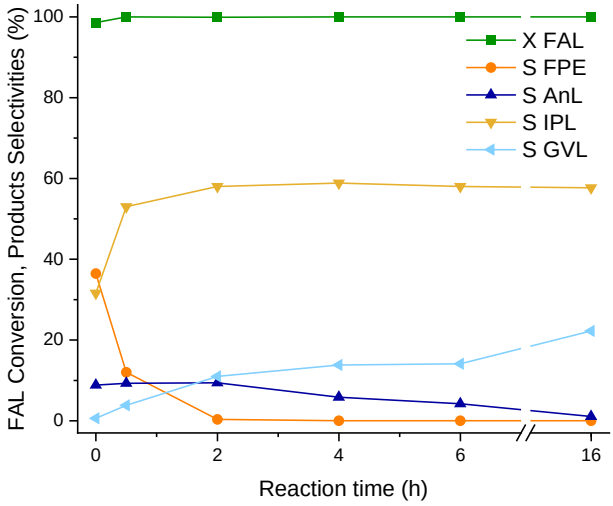

Figure S40. Effect of reaction time on Aq/ZrO_2 30% catalytic performances at 150 °C. Reaction conditions: 1 mmol of FAL; FAL/BAS = 100 mol/mol; 1 eq of water; 15 mL of isopropanol; N_2 pressure of 10 bar.

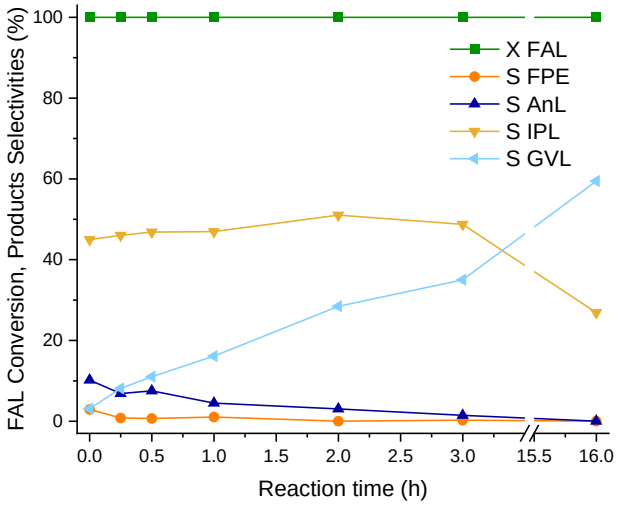

Figure S41. Effect of reaction time on Aq/ZrO_2 30% catalytic performances at 180 °C. Reaction conditions: 1 mmol of FAL; FAL/BAS = 100 mol/mol; 1 eq of water; 15 mL of isopropanol; N_2 pressure of 10 bar.

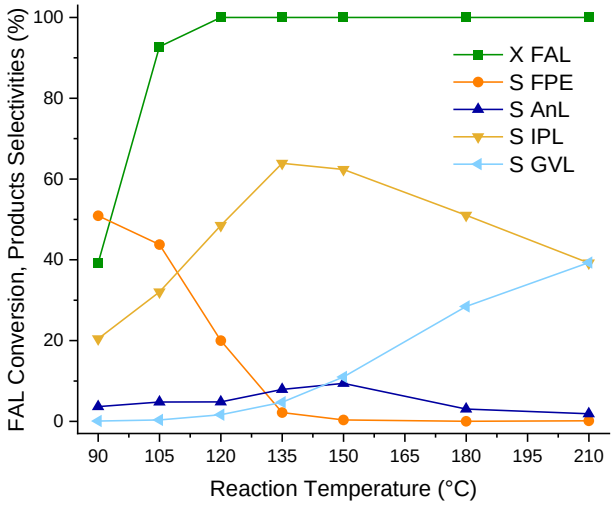

Figure S42. Effect of reaction temperature on Aq/ZrO_2 30% catalytic performances. Reaction conditions: 1 mmol of FAL; FAL/BAS = 100 mol/mol; 1 eq of water; 15 mL of isopropanol; N_2 pressure of 10 bar; Reaction time of 2 h.

An investigation on the initial conversion rate of FAL was carried out at very mild reaction conditions: 5 min at 120 °C, with a catalytic loading of 0.2mol% (FAL/BAS = 500 mol/mol, Figure S43). This highlights that, despite being unable to produce GVL due to the lack of LAS, Aq/SiO_2 30% is more efficient in the conversion of FAL.

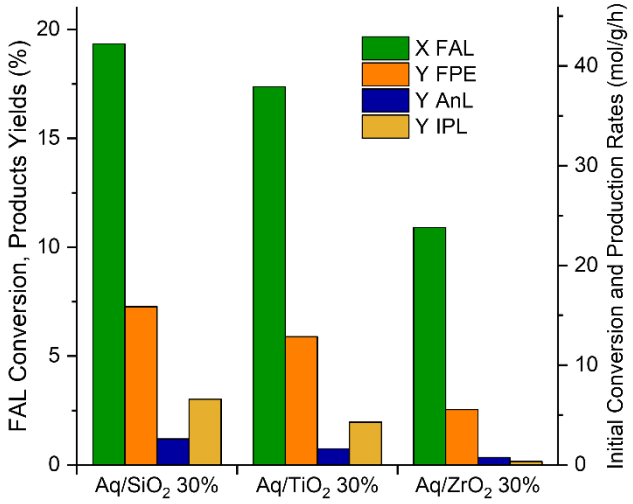

Figure S43. Effect of the oxide on the initial conversion rate of FAL and production rates of the intermediates. Reaction conditions: 1 mmol of FAL; FAL/BAS = 500 mol/mol; 1 eq of water; 15 mL of isopropanol; N_2 pressure of 10 bar; Reaction temperature of 120 °C; Reaction time of 5 min.

The proximity of Brønsted and Lewis acid sites in Aq/ZrO_2 30% is shown to be beneficial in the comparison between its catalytic performance and that of a mixture of Aq/SiO_2 30% (only Brønsted acid) and ZrO_2 (only Lewis acid), reported in Figure S44. The comparison was made keeping Aquivion supported to exclude from this study the effect of the formation of a composite discussed previously (Figure S11).

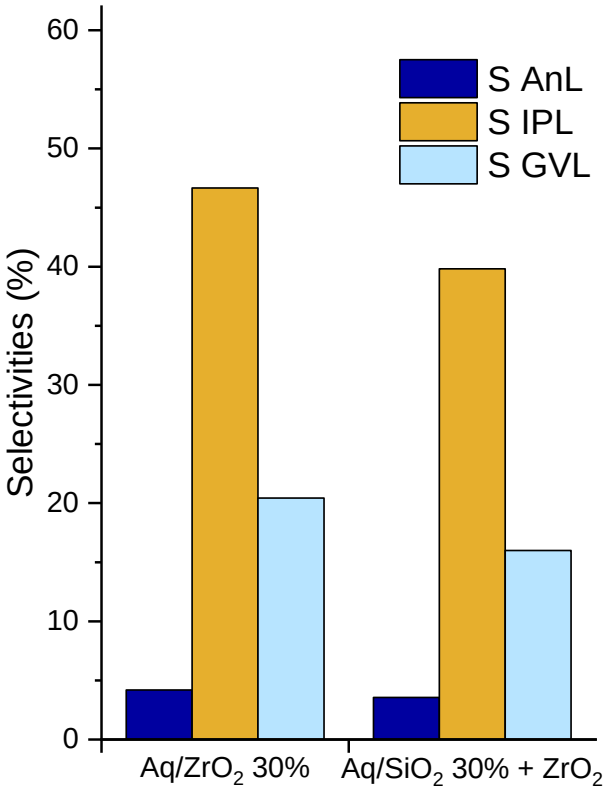

Figure S44. Comparison between Brønsted-Lewis dual acid catalyst and the physical mixture of the two single acid catalysts. Reaction conditions: 1 mmol of FAL; FAL/BAS = 100 mol/mol; FAL/LAS = 100 mol/mol; 1 eq of water; 15 mL of isopropanol; N_2 pressure of 10 bar; Reaction temperature of 180 °C; Reaction time of 2 h. FAL conversion is complete in each test.

To support the ^{15}N MAS NMR spectra of the composites reported in the main document, here are reported the ^{15}N MAS NMR spectra of the oxides (Figure S45), as well as the ^{1}H MAS NMR spectra of both the oxides and the composites before and after isotopically labelled pyridine absorption (respectively, Figure S46 and Figure S47).

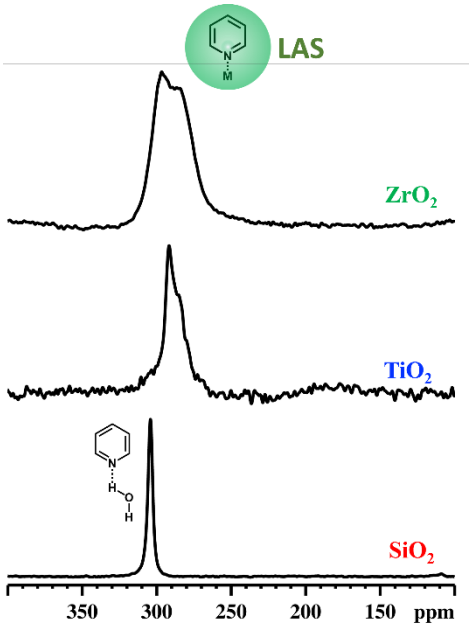

Figure S45. ^{15}N MAS NMR spectra of pure ZrO_2, TiO_2 and SiO_2 supports upon ^{15}N isotopically labelled pyridine adsorption at 25 °C. All samples have been outgassed at 180 °C before pyridine adsorption.

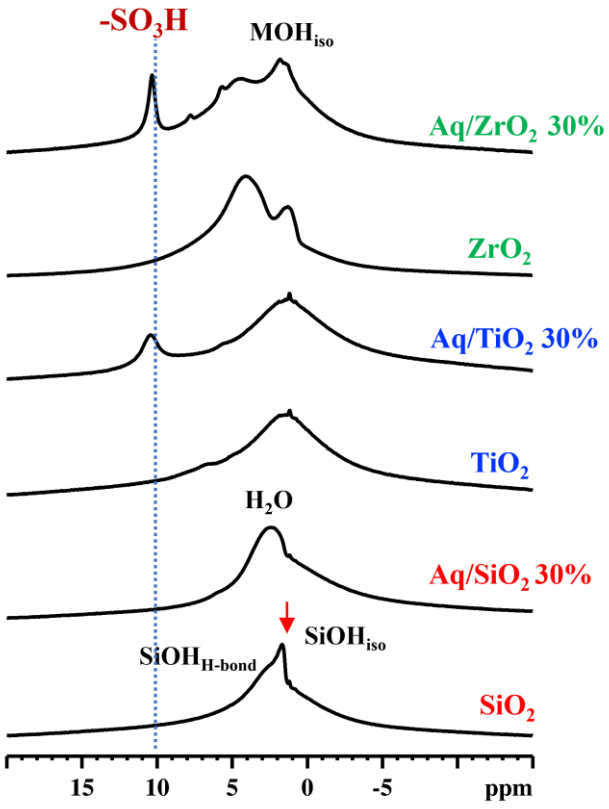

Figure S46. ^{1}H MAS NMR spectra of the Aq/ZrO_2 30%, Aq/TiO_2 30% and Aq/SiO_2 30% in comparison with the pure oxide supports. All samples have been outgassed at 180 °C in vacuum before collecting the spectra.

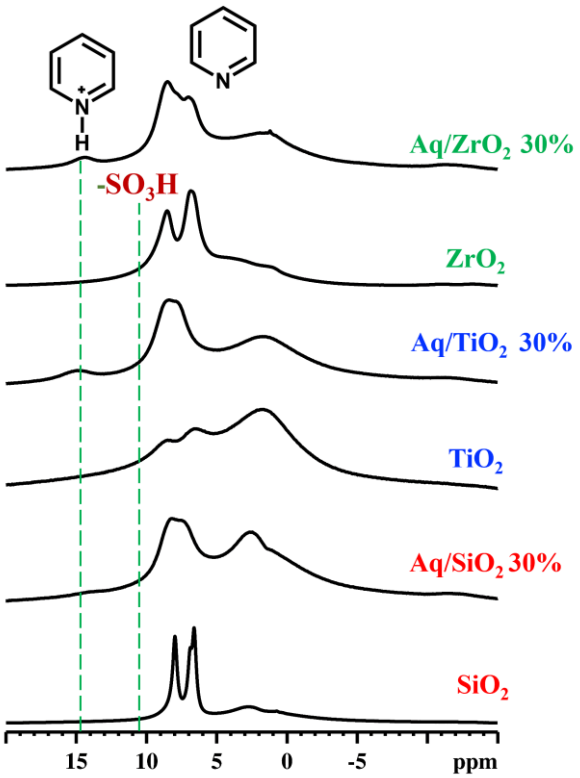

Figure S47. ^{1}H MAS NMR spectra of the Aq/ZrO_2 30%, Aq/TiO_2 30% and Aq/SiO_2 30% with the pure oxide supports upon ^{15}N isotopically labelled pyridine adsorption at 25 °C. All samples have been outgassed at 180 °C before pyridine adsorption.

Study on the effect of the Aquivion content within Aquivion/Zirconia composites

Characterisation

The zirconia-based composites were characterised by means of TGA (Figure S48) revealing polymer contents of 28%, 21% and 10%, very close to the expected values of 30%, 20% and 10%. The porosimetry measurements (Figure S49) of these materials revealed a mesoporous structure and the surface area reported in Table S1.

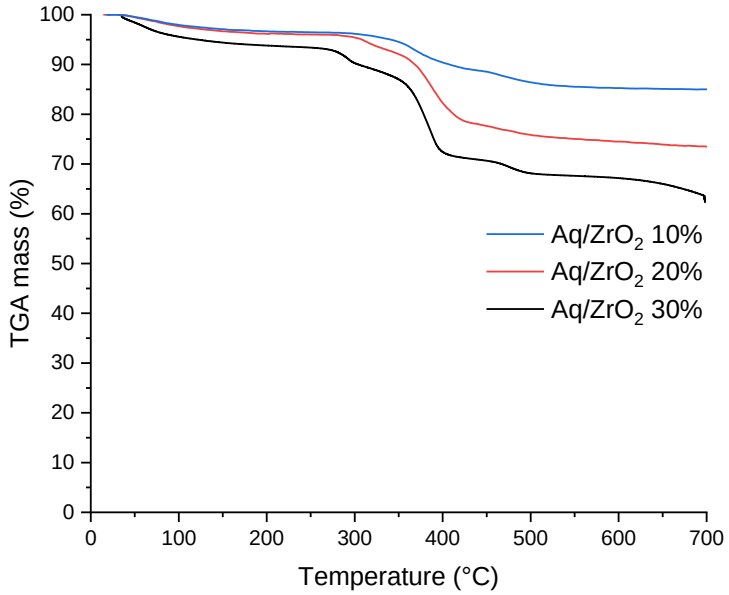

Figure S48. TGA profiles of the Aquivion-Zirconia spray-freeze dried composites at different polymer contents.

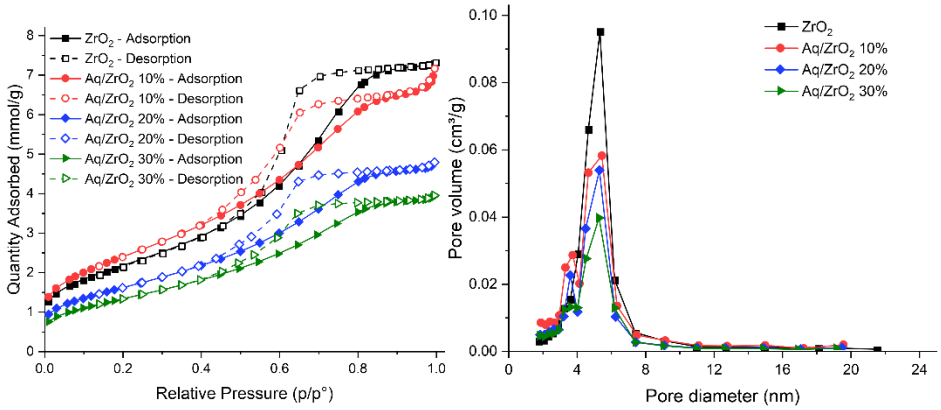

Figure S49. N_2 adsorption/desorption isothermal profiles and pore size distribution of Aquivion-Zirconia spray-freeze dried composites with different polymer contents.

SEM (Figure S50 and Figure S51) and SEM-EDX (Figure S52) once again reveal a granular structure with a good dispersion of the phases.

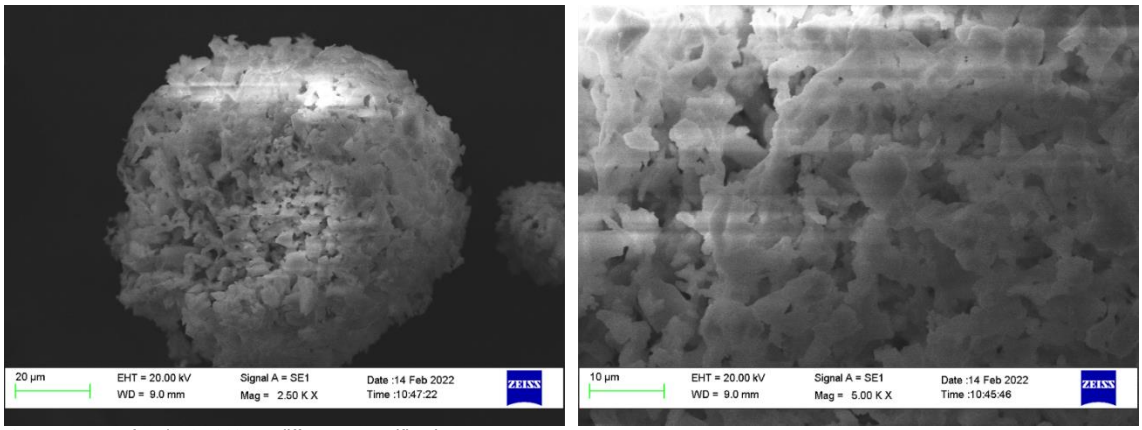

Figure S50. SEM Images of Aq/ZrO_2 20% at different magnifications.

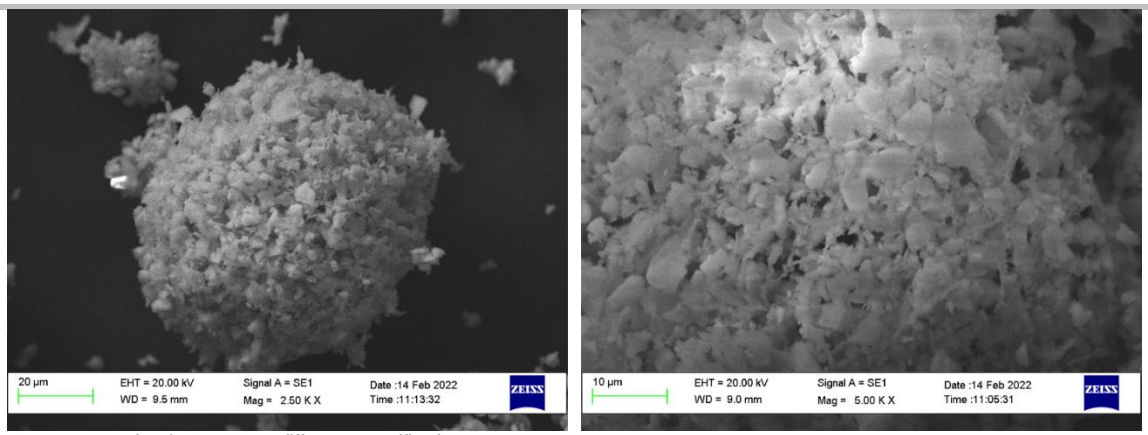

Figure S51. SEM Images of Aq/ZrO_2 10% at different magnifications.

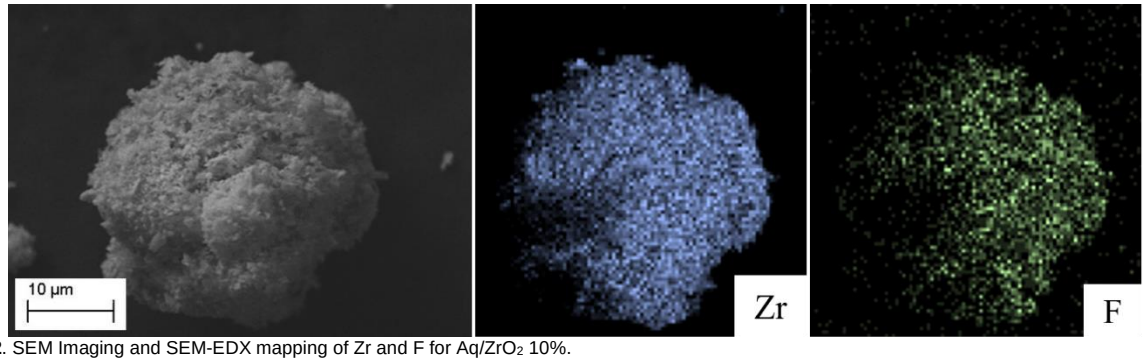

Figure S52. SEM Imaging and SEM-EDX mapping of Zr and F for Aq/ZrO_2 10%.

The ratio between the MAS NMR signal of ^{15}N pyridine absorbed on the Lewis and Brønsted acid sites of the composites (Figure S53) allowed the determination of the LAS/BAS ratio.

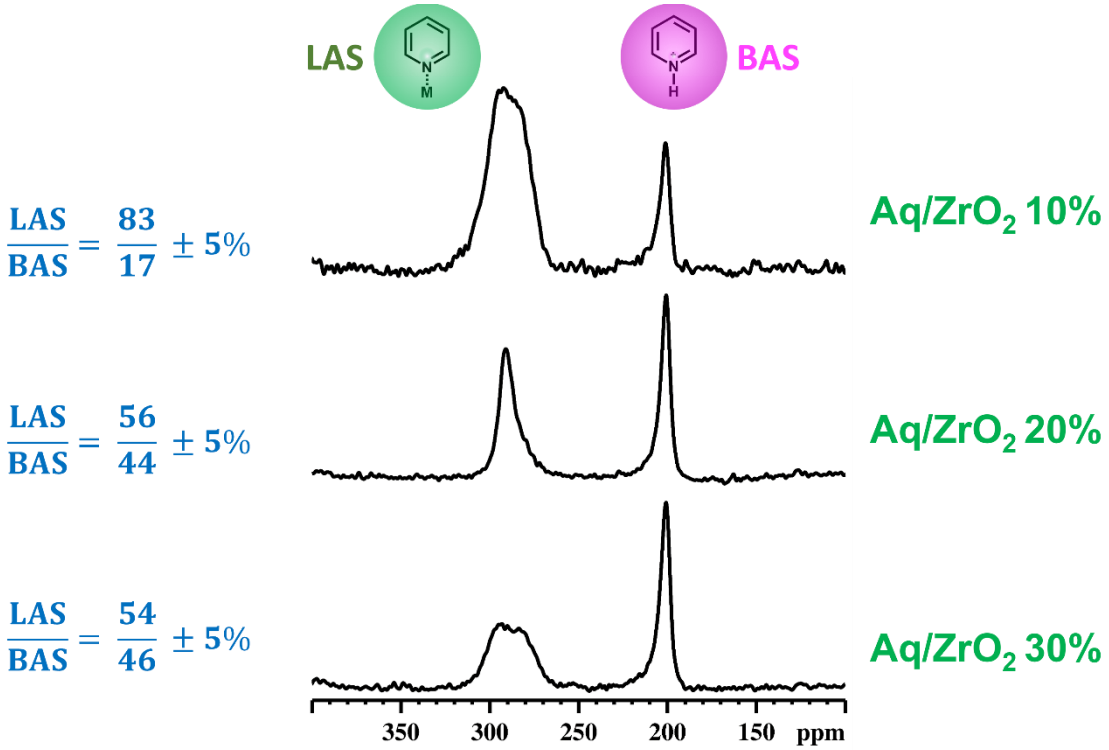

Figure S53.^{15}N MAS NMR spectra of Aq/ZrO_2 30%, Aq/ZrO_2 20%, and Aq/ZrO_2 10% upon ^{15}N isotopically labelled pyridine adsorption at 25 °C. All samples have been outgassed at 180 °C before pyridine adsorption.

Catalytic testing

The comparison between the catalytic performance of the three zirconia-based composites (Figure S54) shows that an increase in Lewis acidity leads to the expected increase in GVL selectivity, accompanied by a decrease in IPL and AnL selectivities.

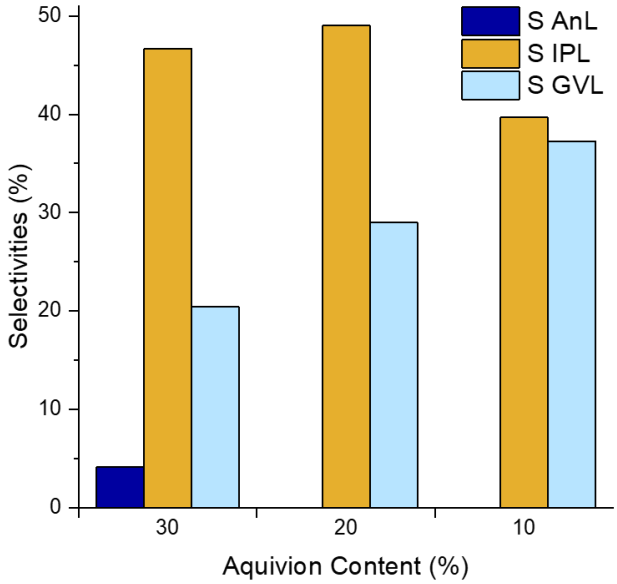

Figure S54. Effect of the Aquivion content within Aq/ZrO_2 composite materials. Reaction conditions: 1 mmol of FAL; FAL/BAS = 100 mol/mol; 1 eq of water; 15 mL of isopropanol; N_2 pressure of 10 bar; Reaction temperature of 180 °C; Reaction time of 2 h. FAL conversion is complete in each test.

TGA profiles of the spent catalysts (Figure S55) show a consistent increase in weight loss when compared to the respective fresh catalysts. This suggests that deactivation of the catalysts might be attributed to fouling more than leaching of the polymer.

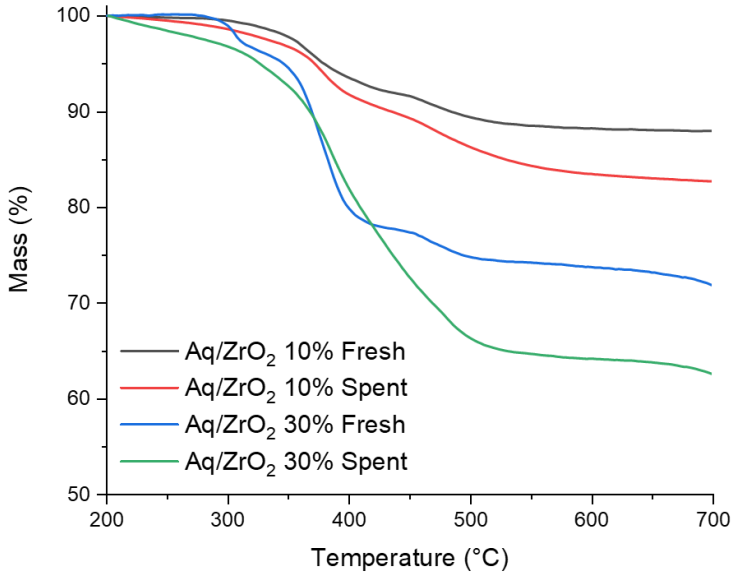

Figure S55. TGA profiles of Aquivion-Zirconia spray-freeze dried composites before and after catalytic tests. Each profile was normalized at 200 °C to remove the effect of adsorbed solvent or humidity.

The effect of catalytic loading for the three zirconia-based composites is reported in Figures S55-S57. Generally speaking, it can be observed that the BAS-promoted steps are completely carried out in all but the most extreme conditions (FAL/BAS = 500 for Aq/ZrO_2 10%, the catalyst with the lowest amount of BAS), demonstrating the outstanding catalytic activity of Aquivion.

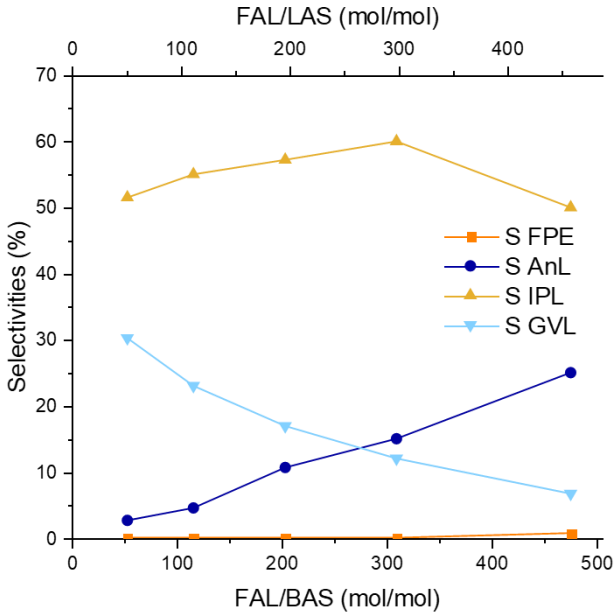

Figure S56. Effect of the catalyst amount on the reaction outcome with Aq/ZrO_2 30% as a catalyst. On the horizontal axes are reported the molar ratio between the substrate (FAL) and either Brønsted acidity (BAS) or Lewis acidity (LAS). Reaction conditions: 1 mmol of FAL; 1 eq of water; 15 mL of isopropanol; N_2 pressure of 10 bar; Reaction temperature of 180 °C; Reaction time of 2 h. FAL conversion is complete in each test.

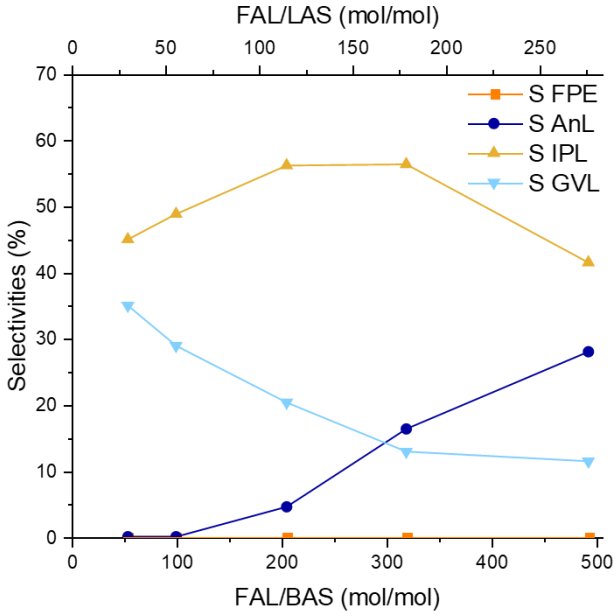

Figure S57. Effect of the catalyst amount on the reaction outcome with Aq/ZrO_2 20% as a catalyst. On the horizontal axes are reported the molar ratio between the substrate (FAL) and either Brønsted acidity (BAS) or Lewis acidity (LAS). Reaction conditions: 1 mmol of FAL; 1 eq of water; 15 mL of isopropanol; N_2 pressure of 10 bar; Reaction temperature of 180 °C; Reaction time of 2 h. FAL conversion is complete in each test.

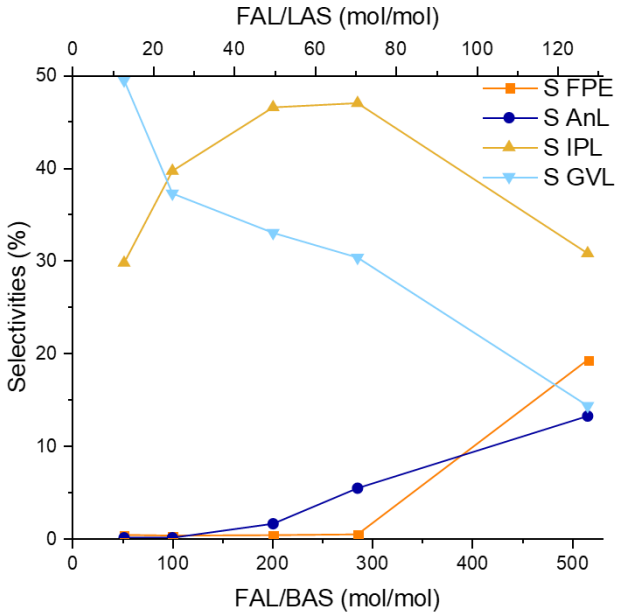

Figure S58. Effect of the catalyst amount on the reaction outcome with Aq/ZrO_2 10% as a catalyst. On the horizontal axes are reported the molar ratio between the substrate (FAL) and either Brønsted acidity (BAS) or Lewis acidity (LAS). Reaction conditions: 1 mmol of FAL; 1 eq of water; 15 mL of isopropanol; N_2 pressure of 10 bar; Reaction temperature of 180 °C; Reaction time of 2 h. FAL conversion is complete in each test.

Reusability tests were carried out on Aq/ZrO_2 30% and Aq/ZrO_2 10% (Figure S59), highlighting the better resistance to deactivation of Aq/ZrO_2 30%. MAS NMR spectra (Figures S59-S61) also support the previously presented TGA profiles (Figure S55) in attributing deactivation of these materials to fouling, in particular to the deposition of carbonaceous compounds on the BAS.

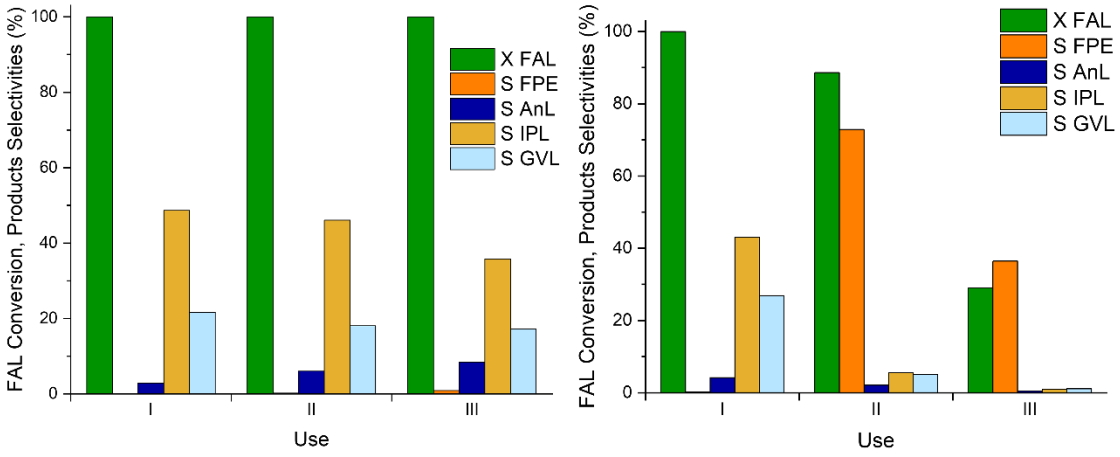

Figure S59. Reusability tests on Aq/ZrO_2 30% (Left) and Aq/ZrO_2 10% (Right). Reaction conditions: 1 mmol of FAL; FAL/BAS = 100 mol/mol; 1 eq of water; 15 mL of isopropanol; N_2 pressure of 10 bar; Reaction temperature of 180 °C; Reaction time of 2 h.

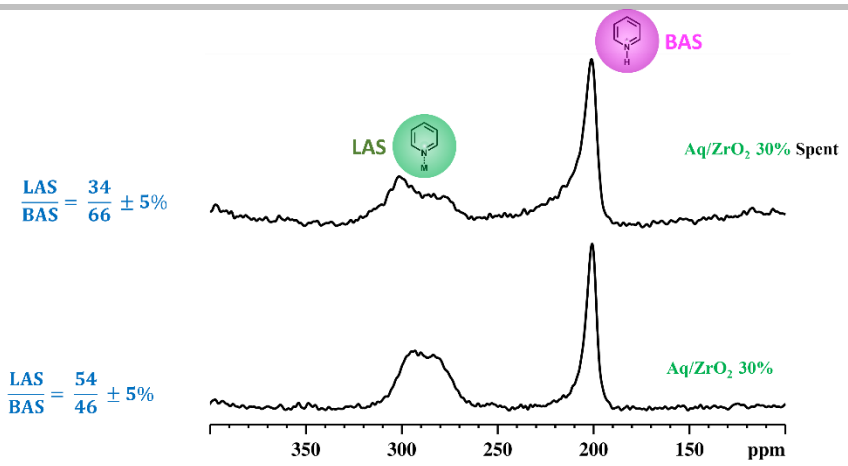

Figure S60. ^{15}N MAS NMR spectra of Aq/ZrO_2 30%, before and after (Spent) catalytic testing upon ^{15}N isotopically labelled pyridine adsorption at 25 °C. All samples have been outgassed at 180 °C before pyridine adsorption.

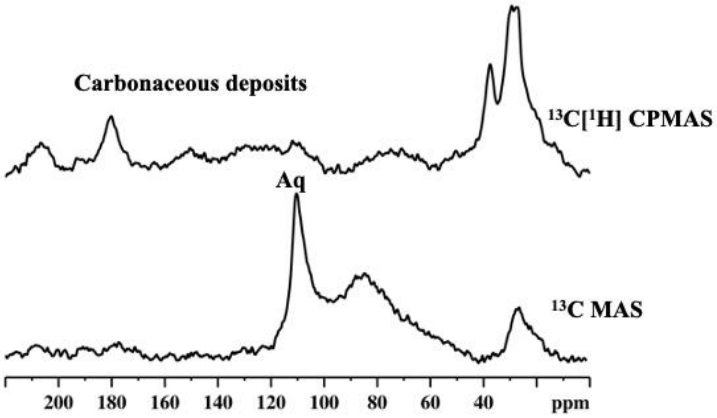

Figure S61. ^{13}C MAS and CPMAS NMR of Aq/ZrO_2 30% Spent catalyst.

.

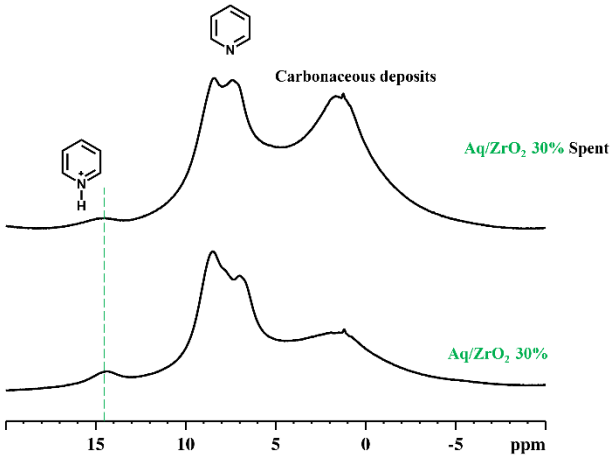

Figure S62. ^{1}H MAS NMR spectra of Aq/ZrO_2 30%, before and after (Spent) catalytic testing upon ^{15}N isotopically labelled pyridine adsorption at 25 °C. All samples have been outgassed at 180 °C before pyridine adsorption.

SUPPORTING INFORMATION

Mechanistic Studies

Table S3. Catalytic tests carried out for the investigation of the reaction mechanism. Reaction conditions: 1 mmol of FU; FU/BAS = 100 mol/mol (when Aquivion is present in the catalyst; in the case of zirconia, the catalyst weight is 25mg); 1 eq of water; 15 mL of isopropanol; N_2 pressure of 10 bar.

Entry	Substrate	Temperature (°C)	Time (h)	Catalyst	Conv. (%)	Selectivity (%)				
						FAL	FPE	AnL	IPL	GVL
1	FU	150	2	ZrO_2	61	88	1	0	0	0
2	FU	150	2	Aq/ZrO_2 10%	46	5	48	7	31	5
3	FU	150	2	Aq/ZrO_2 30%	50	3	48	13	15	4
4	FU	180	2	ZrO_2	98	58	1	0	0	0
5	FU	180	2	Aq/ZrO_2 10%	86	4	32	5	15	10
6	FU	180	2	Aq/ZrO_2 30%	80	0	1	5	43	25
7	FAL	150	2	Aq/ZrO_2 10%	99	-	15	12	61	8
8	FAL	150	2	Aq/ZrO_2 30%	100	-	5	11	54	2
9	FAL	180	2	Aq/ZrO_2 10%	100	-	1	4	36	19
10	FAL	180	2	Aq/ZrO_2 30%	100	-	0	14	49	8
11	FEE	150	2	Aq/ZrO_2 10%	85	-	14	16	54	8
12	FEE	150	2	Aq/ZrO_2 30%	93	-	5	15	51	2
13	FEE	180	2	Aq/ZrO_2 10%	99	-	1	4	38	27
14	FEE	180	2	Aq/ZrO_2 30%	99	-	1	18	46	12
15	FEE	180	0	Aq/ZrO_2 10%	19	-	73	2	8	0
16	FEE	180	0.25	Aq/ZrO_2 10%	54	-	64	5	18	0
17	FEE	180	0.5	Aq/ZrO_2 10%	70	-	54	4	25	1
18	FEE	180	1	Aq/ZrO_2 10%	82	-	40	10	35	2
19	AnL	150	2	ZrO_2	58	-	-	-	8	24
20	AnL	150	2	Aq/ZrO_2 10%	93	-	-	-	18	12
21	AnL	150	2	Aq/ZrO_2 30%	96	-	-	-	27	3
22	AnL	180	2	ZrO_2	87	-	-	-	9	57
23	AnL	180	2	Aq/ZrO_2 10%	95	-	-	-	28	71
24	AnL	180	2	Aq/ZrO_2 30%	98	-	-	-	51	12
25	PrL	150	2	ZrO_2	44	-	-	0	5	39
26	PrL	150	2	Aq/ZrO_2 10%	8	-	-	6	21	74
27	PrL	150	2	Aq/ZrO_2 30%	3	-	-	26	42	32
28	PrL	180	2	ZrO_2	88	-	-	0	3	39
29	PrL	180	2	Aq/ZrO_2 10%	42	-	-	0	8	56
30	PrL	180	2	Aq/ZrO_2 30%	8	-	-	5	30	65
31	PrL	210	2	ZrO_2	97	-	-	0	2	74
32	PrL	210	2	Aq/ZrO_2 10%	84	-	-	0	5	84
33	PrL	210	2	Aq/ZrO_2 30%	22	-	-	0	19	55

Figures S62-S68 represent the reactions carried out on Aq/ZrO_2 10% and Aq/ZrO_2 30% (as well as pure ZrO_2 for the LAS-converted substrates) starting from different intermediates of the reaction, in order to understand the reaction mechanism. Each reaction was carried out both at 150 °C (left) and 180 °C (right). Due to the low conversions, the reaction starting from Propyl Levulinate (PrL, the commercially available analogue to IPL, Figure S66) was also carried out at 210 °C (Figure S67).

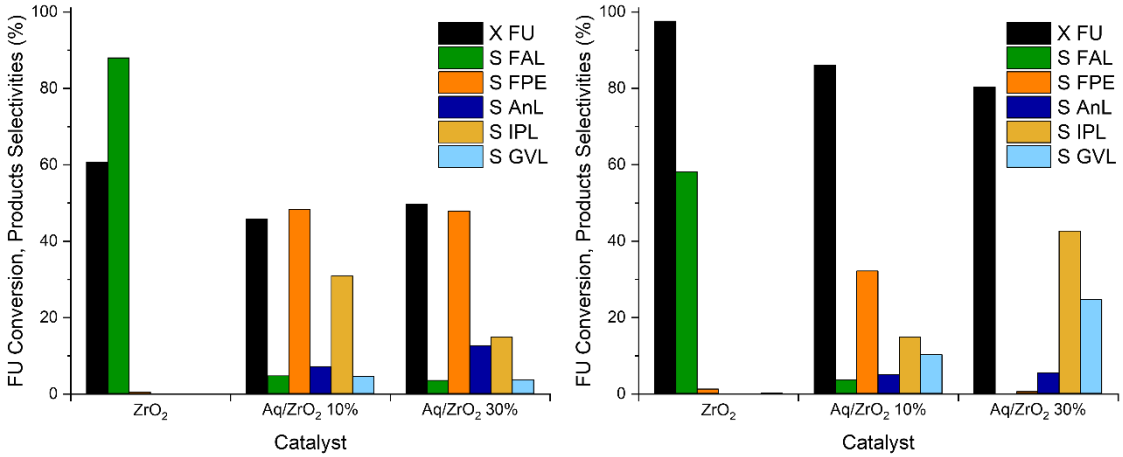

Figure S63. Effect of the catalyst composition on its performance using Furfural (FU) as substrate. Reaction conditions: 1 mmol of FU; FU/BAS = 100 mol/mol (when Aquivion is present in the catalyst; in the case of zirconia, the catalyst weight is 25mg); 1 eq of water; 15 mL of isopropanol; N_2 pressure of 10 bar; Reaction temperature of 150 °C (left) and 180 °C (right); Reaction time of 2 h.

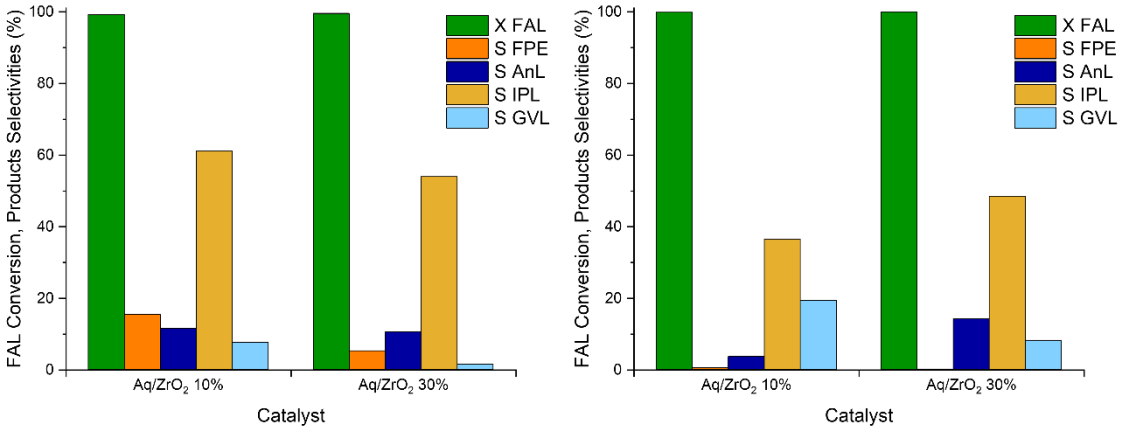

Figure S64. Effect of the catalyst composition on its performance using Furfuryl Alcohol (FAL) as substrate. Reaction conditions: 1 mmol of FAL; FAL/BAS = 100 mol/mol; 1 eq of water; 15 mL of isopropanol; N_2 pressure of 10 bar; Reaction temperature of 150 °C (left) and 180 °C (right); Reaction time of 2 h.

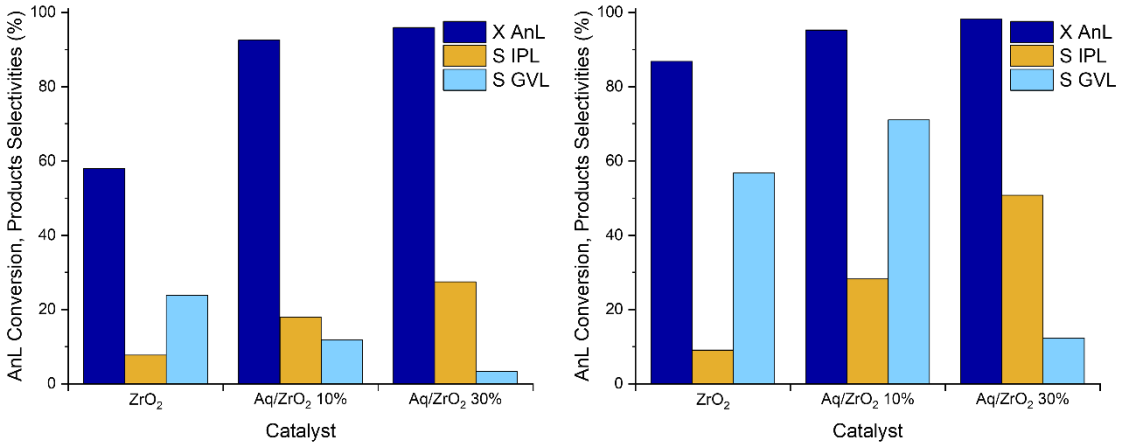

Figure S65. Effect of the catalyst composition on its performance using Angelica Lactone (AnL) as substrate. Reaction conditions: 1 mmol of AnL; AnL/BAS = 100 mol/mol (when Aquivion is present in the catalyst; in the case of zirconia, the catalyst weight is 25mg); 1 eq of water; 15 mL of isopropanol; N_2 pressure of 10 bar; Reaction temperature of 150 °C (left) and 180 °C (right); Reaction time of 2 h.

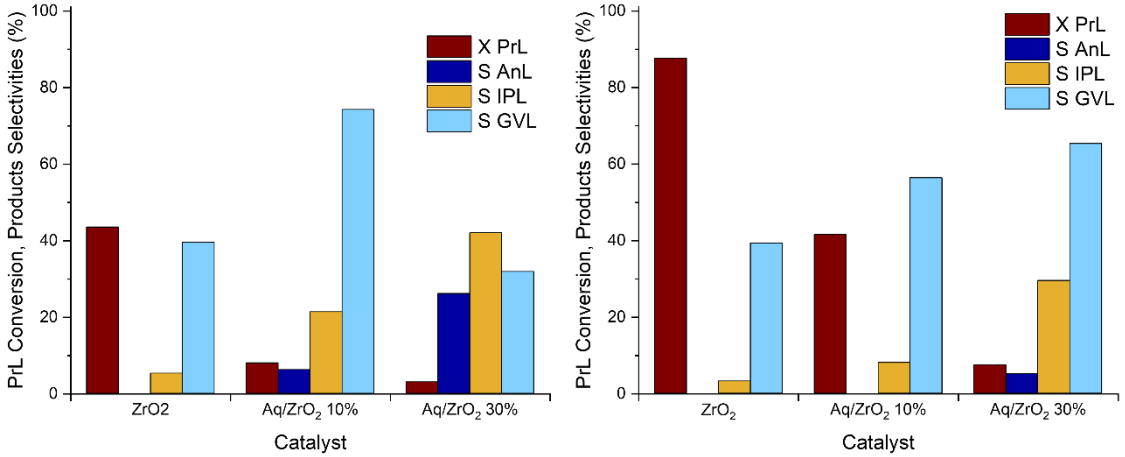

Figure S66. Effect of the catalyst composition on its performance using Propyl Levulinate (PrL) as substrate. Reaction conditions: 1 mmol of PrL; PrL/BAS = 100 mol/mol (when Aquivion is present in the catalyst; in the case of zirconia, the catalyst weight is 25mg); 1 eq of water; 15 mL of isopropanol; N_2 pressure of 10 bar; Reaction temperature of 150 °C (left) and 180 °C (right); Reaction time of 2 h.

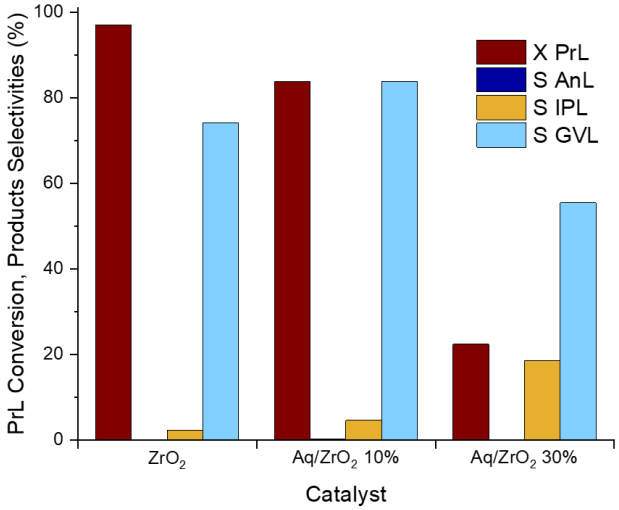

Figure S67. Effect of the catalyst composition on its performance using Propyl Levulinate (PrL) as substrate. Reaction conditions: 1 mmol of PrL; PrL/BAS = 100 mol/mol (when Aquivion is present in the catalyst; in the case of zirconia, the catalyst weight is 25mg); 1 eq of water; 15 mL of isopropanol; N_2 pressure of 10 bar; Reaction temperature of 210 °C; Reaction time of 2 h.

Furfuryl Ethyl Ether (FEE) was employed in Figure S68 as a commercially available substitute for FPE. It can be observed that its conversion never leads to its hydrolytic ring opening product, ethyl levulinate, EL. Instead, IPL can be observed, which is the hydrolytic ring opening product of FPE. FPE is also observed at 150 °C in significant amounts. To better elucidate this strange behaviour leading to a change in ether group, a study at different reaction times was carried out and is reported in Figure S69. From this study it can be observed that FPE is indeed the first product obtained from FEE conversion, and only after that first step does hydrolytic ring opening take place, leading to IPL instead of EL.

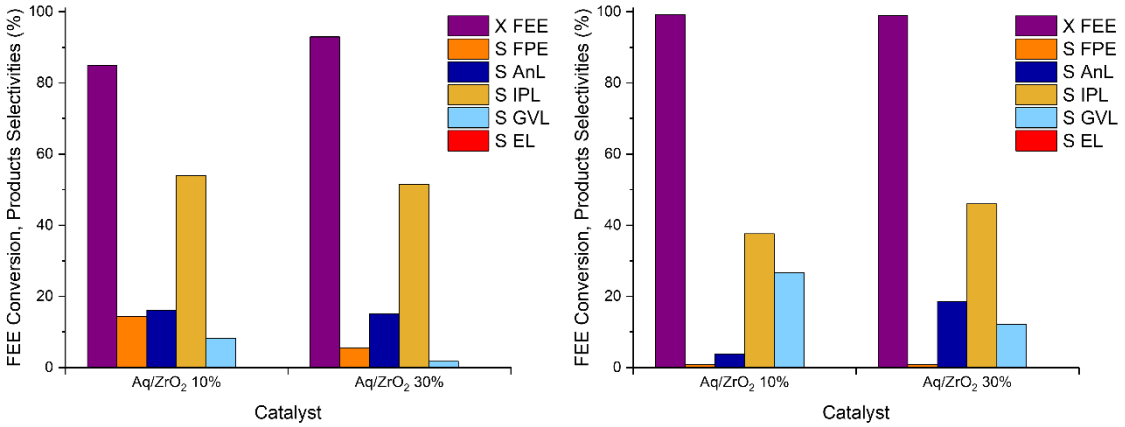

Figure S68. Effect of the catalyst composition on its performance using Furfuryl Ethyl Ether (FEE) as substrate. Reaction conditions: 1 mmol of FEE; FEE/BAS = 100 mol/mol; 1 eq of water; 15 mL of isopropanol; N_2 pressure of 10 bar; Reaction temperature of 150 °C (left) and 180 °C (right); Reaction time of 2 h.

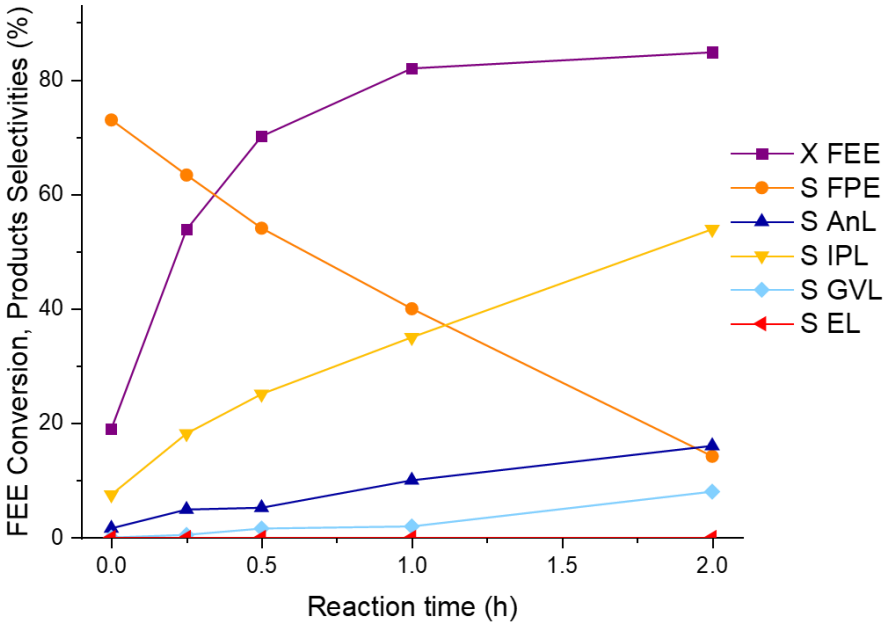

Figure S69. Effect of reaction time on the products selectivities starting from FEE over Aq/ZrO_2 10%. Reaction conditions: 1 mmol of FEE; FEE/BAS = 100 mol/mol; 1 eq of water; 15 mL of isopropanol; N_2 pressure of 10 bar; Reaction temperature of 180 °C.

To explain this "transetherification", the mechanism in Figure S70 is proposed, wherein the expected hydrolytic ring opening of FEE highlighted in red does not take place. Instead, the acidity of the catalysts promotes the elimination of ethanol from the molecule according to the process highlighted in green, leading to intermediate **1** (2-methylene-2H-furan-1-ium), which undergoes addition of isopropanol, the solvent. After that, the reaction in yellow takes place, leading to the hydrolytic ring opening of FPE to IPL and then the reduction of IPL to lead to GVL.

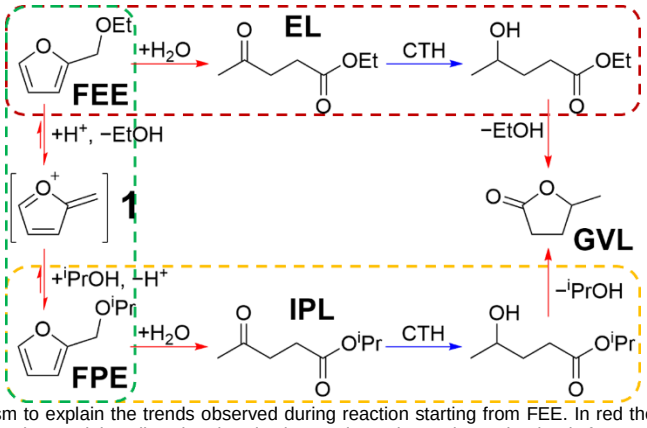

Figure S70. Proposed reaction mechanism to explain the trends observed during reaction starting from FEE. In red the reaction pathway that would lead to the formation of ethyl levulinate (EL) and is not observed; in yellow the already observed reaction pathway that leads from FPE (the first product obtained from FEE) to IPL and then GVL; in green, the proposed reaction pathway that explains the conversion of FEE into FPE and the observed selectivity trends.

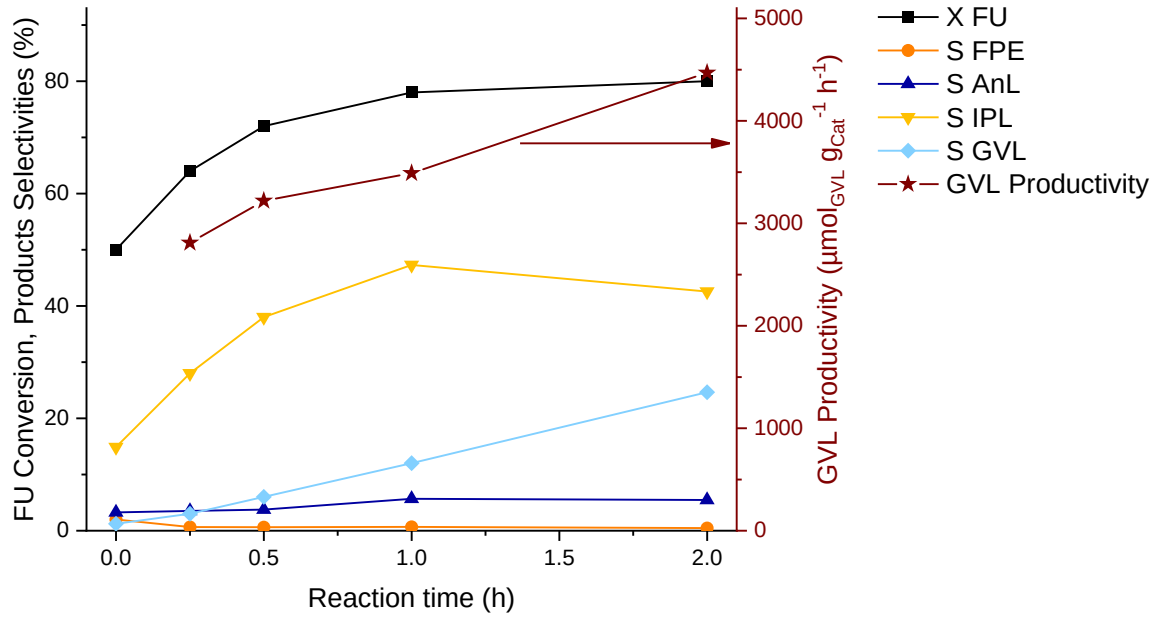

Figure S71. Effect of reaction time on the reaction outcome starting from FU. Reaction conditions: 1 mmol of FU; catalyst Aq/ZrO_2 30%; FU/BAS = 100 mol/mol; 1 eq of water; 15 mL of isopropanol; N_2 pressure of 10 bar; Reaction temperature of 180 °C.

Table S4. Comparison between the GVL productivity achieved in this work in comparison to the results published in literature for similar cascade reactions. Entry 14 refers to the GVL productivity achieved starting from Furfural, Entry 6 of Table S1.

Entry	Catalyst	Reaction Temperature (°C)	GVL Productivity (μmol_{GVL} g_{Cat}^{-1} h^{-1})	Reference
1	Sulfated ZrO_2	150	2200	[6]
2	Zr-Mont	160	680	[7]
3	5% Hf-Al-USY	140	540	[8]
4	Zr-Al-SCM	170	340	[9]
5	Zr-Al-Beta	170	350	[10]
6	HZ-ZrP	185	340	[11]
7	VPA–Hf	180	290	[12]
8	Fe_3O_4/ZrO_2@MCM-41	150	420	[13]
9	ZrO_2-[Al]MFI-NS	170	580	[14]
10	Zr-KIT	180	1480	[15]
11	DUT-67(Hf)	180	370	[16]
12	HPW/Zr-Beta	160	280	[17]
13	ZrO_2-SBA-15	170	1430	[18]
14	Aq/ZrO_2 30%	150	360	This work
15	Aq/ZrO_2 30%	180	4470	This work

References

[1] L. Ghassemzadeh, M. Marrony, R. Barrera, K. D. Kreuer, J. Maier, K. Müller, *J. Power Sources* **2009**, *186*, 334–338.

[2] S. Andreoli, C. Oldani, V. Fiorini, S. Stagni, G. Fornasari, S. Albonetti, *Appl. Catal. Gen.* **2020**, *597*, 117544.

[3] H. G. Bernal, C. Oldani, T. Funaioli, A. M. Raspolli Galletti, *New J. Chem.* **2019**, *43*, 14694–14700.
[4] H. Gómez Bernal, P. Benito, E. Rodríguez-Castellón, A. M. Raspolli Galletti, T. Funaioli, *Appl. Catal. Gen.* **2019**, *575*, 111–119.
[5] G. M. G. Maldonado, R. S. Assary, J. A. Dumesic, L. A. Curtiss, *Energy Environ. Sci.* **2012**, *5*, 8990–8997.
[6] A. Merenda, S. A. Orr, Y. Liu, B. Hernández Garcia, A. Osatiashtiani, G. Morales, M. Paniagua, J. A. Melero, A. F. Lee, K. Wilson, *ChemCatChem* **2023**, *15*, e202201224.
[7] P. Zhang, M. Ma, P. Hou, J. Cao, Q. Guo, H. Yue, G. Tian, S. Feng, *Mol. Catal.* **2023**, *535*, 112832.
[8] B. Tang, S. Li, W.-C. Song, Y. Li, E.-C. Yang, *Sustain. Energy Fuels* **2021**, *5*, 4724–4735.
[9] X. Li, X. Yuan, G. Xia, J. Liang, C. Liu, Z. Wang, W. Yang, *J. Catal.* **2020**, *392*, 175–185.
[10] J. A. Melero, G. Morales, J. Iglesias, M. Paniagua, C. López-Aguado, *Ind. Eng. Chem. Res.* **2018**, *57*, 11592–11599.
[11] L. Ye, Y. Han, H. Bai, X. Lu, *ACS Sustain. Chem. Eng.* **2020**, *8*, 7403–7413.
[12] J. Tan, Y. Liu, M. Li, H. Li, S. Yang, *Sustain. Energy Fuels* **2022**, *6*, 484–501.
[13] X. Gao, X. Yu, L. Peng, L. He, J. Zhang, *Fuel* **2021**, *300*, 120996.
[14] K. D. Kim, J. Kim, W. Y. Teoh, J.-C. Kim, J. Huang, R. Ryoo, *RSC Adv.* **2020**, *10*, 35318–35328.
[15] J. He, H. Li, Y. Xu, S. Yang, *Renew. Energy* **2020**, *146*, 359–370.
[16] W. Li, Z. Cai, H. Li, Y. Shen, Y. Zhu, H. Li, X. Zhang, F. Wang, *Mol. Catal.* **2019**, *472*, 17–26.
[17] H. P. Winoto, Z. A. Fikri, J.-M. Ha, Y.-K. Park, H. Lee, D. J. Suh, J. Jae, *Appl. Catal. B Environ.* **2019**, *241*, 588–597.
[18] J. Iglesias, J. A. Melero, G. Morales, J. Moreno, Y. Segura, M. Paniagua, A. Cambra, B. Hernández, *Catalysts* **2015**, *5*, 1911–1927.

Author Contributions

Dr. A. Allegri: Catalytic testing, writing of draft; A. Saotta and F. Liuzzi: Catalytic testing, TEM imaging; Prof. E. Gianotti and Dr. G. Paul: ^{1}H, ^{13}C and ^{15}N MAS NMR spectroscopy; Dr. A. S. Cattaneo and Dr. C. Oldani: ^{19}F MAS NMR; A. Brigliadori and Dr. I. Zanoni: ζ-potential measurements, catalyst synthesis and SEM imaging; Dr. G. Fornasari: Data revision, N_2 porosimetry; Prof. N. Dimitratos: Data and draft revisions; Prof. S. Albonetti: Data revision, project coordination.